An *in vivo,* neuron-specific approach for pairing translational and epigenetic signatures of early-life exercise.

Raus AM*[1], Fuller TD*[2], Nelson NE*[1], Bayat A[2], Valientes SDA[2], Ivy AS[1,2,3,4]

*These authors contributed equally to the work.

[1]Department of Physiology and Biophysics,
[2]Department of Pediatrics University of California- Irvine School of Medicine, Irvine, CA,

[3]Department of Anatomy and Neurobiology University of California- Irvine School of Medicine, Irvine, CA,
University of California- Irvine School of Medicine, Irvine, CA

[4]Division of Neurology, Children's Hospital Orange County, Orange, CA

Correspondence to aivy@hs.uci.edu

Abstract

Aerobic exercise promotes physiological and molecular adaptations in neurons to influence brain function and behavior. The most well studied neurobiological consequences of exercise are those which underlie exercise-induced improvements in hippocampal memory, including the expression and regulation of the neurotrophic factor *Bdnf*. Whether aerobic exercise taking place during early-life periods of postnatal brain maturation has similar impacts on gene expression and its regulation remains to be investigated. Using unbiased next-generation sequencing we characterize gene expression programs and their regulation by specific, memory-associated histone modifications during juvenile-adolescent voluntary exercise (ELE). Traditional transcriptomic and epigenomic sequencing approaches have either used heterogeneous cell populations from whole tissue homogenates or flow cytometry for single cell isolation to distinguish cell types / subtypes. These methods fall short in providing cell-type specificity without compromising sequencing depth or procedure-induced changes to cellular phenotype. In this study, we use simultaneous isolation of translating mRNA and nuclear chromatin from a neuron-enriched cell population to more accurately pair ELE-induced changes in gene expression with epigenetic modifications. We employ a line of transgenic mice expressing the NuTRAP (Nuclear Tagging and Translating Ribosome Affinity Purification) cassette under the *Emx1* promoter allowing for brain cell-type specificity. We then developed a technique that combines nuclear isolation using Isolation of Nuclei TAgged in Specific Cell Types (INTACT) with Translating Ribosomal Affinity Purification (TRAP) methods to determine cell type-specific epigenetic modifications influencing gene expression programs from a population of *Emx1* expressing hippocampal neurons. Data from RNA-seq and CUT&RUN-seq were coupled to evaluate histone modifications influencing the expression of translating mRNA in neurons after early-life exercise (ELE). We also performed separate INTACT and TRAP isolations for validation of our protocol and demonstrate similar molecular functions and biological processes implicated by gene ontology (GO) analysis. Finally, as prior studies use tissue from opposite brain hemispheres to pair transcriptomic and epigenomic data from the same rodent, we

take a bioinformatics approach to compare hemispheric differences in gene expression programs and histone modifications altered by by ELE. Our data reveal transcriptional and epigenetic signatures of ELE exposure and identify novel candidate gene-histone modification interactions for further investigation. Importantly, our novel approach of combined INTACT/TRAP methods from the same cell suspension allows for simultaneous transcriptomic and epigenomic sequencing in a cell-type specific manner.

Introduction

Environmental experiences engage epigenetic mechanisms to modulate gene expression and cell function in post-mitotic neurons [1, 2]. Histone modifications and DNA methylation are particularly important for neuronal adaptation to environmental signals by altering gene transcription and synaptic function [3, 4]. Behavioral outputs such as stress susceptibility, reward seeking, and long-term memory have been shown to result from changes to chromatin accessibility and gene expression in neurons [5-9]. In addition to this, the neuronal chromatin landscape undergoes waves of epigenetic modifications as a function of brain maturation itself [10-12]. Postnatal periods of heightened sensitivity to environmental stimuli can lead to lasting changes to cellular function, and may result from temporally specific epigenetic mechanisms in the developing brain [13, 14]. How epigenetic mechanisms in postmitotic neurons are influenced by early-life experiences to inform long-term function is beginning to be explored. Identifying gene regulatory mechanisms involved in modulating cell function during sensitive windows of brain development can aid in understanding how early-life experiences inform long-term behavioral outcomes.

Aerobic exercise has generally been found to enhance performance on cognitive tasks involving the hippocampus in both adult humans and animal models [15, 16]. The type, timing, and duration of exercise exposure matters with regard to whether it has persistent impact on hippocampal function [17-19]. Findings in rodents demonstrate that voluntary exercise exposure or treatment with HDAC3 inhibition improves hippocampal memory function [20-22]. Although the majority of these studies have been performed in adults, more recent work suggests that the effects of exercise on hippocampal memory and the associated alterations in neurotrophic factor expression, synaptic plasticity, and neurogenesis are similar in juvenile and adolescent periods [17, 23-26]. Previous work in our lab showed that voluntary wheel running for either one week (postnatal days (P) 21-27) or three weeks (P21-41) led to enabled hippocampal long-term memory (LTM) in response to a subthreshold learning experience when tested on P42. This was associated with increased CA1 LTP in the three-week exercise group, as well as modulations to CA1

synaptic physiology in both the one-week and three-week exercisers [17]. Notably, the effects of exercise during P21-27 lasted at least two weeks after exercise cessation, which may be longer than the influence of exercise on adult hippocampal function [27]. This finding suggests that exercise exposure during a sensitive period of postnatal hippocampal development has the potential to persistently impact hippocampal function.

The goal of this study is to identify novel programs of neuronal gene expression and their epigenetic regulation resulting from exercise during early life. In order to do this, we developed a transgenic mouse line and experimental protocol to simultaneously obtain epigenetic and transcriptional information from *Emx1*-expressing neurons of the hippocampus. By crossing the Emx1- *Cre* transgenic line with mice expressing the NuTRAP (Nuclear Tagging and Translating Ribosome Affinity Purification [28]) cassette (termed Emx1-NuTRAP mice) we are able to simultaneously isolate whole nuclei and translating mRNA from a neuron-enriched population of cells. Using the same tissue sample, we combine the first steps of the INTACT (Isolation of Nuclei TAgged in specific Cell Types[29]) and TRAP (Translating Ribosomal Affinity Purification [30]) protocols and obtain high-quality DNA and RNA yields for downstream sequencing procedures. Juvenile Emx1-NuTRAP mice underwent three weeks of early-life exercise during P21-41 (hereafter referred to as "ELE") in order to determine the epigenetic regulation of exercise-induced changes to gene expression and cell function. Using novel technical approaches, this study uncovers hippocampal gene expression programs and associated histone modifications that are driven by voluntary wheel running during the juvenile and adolescent developmental periods.

Results

"Emx1-NuTRAP" mouse allows for simultaneous isolation of nuclear chromatin and translating mRNA from a single population of hippocampal neurons.

Our goal was to obtain translating mRNA and nuclear DNA from a single population of neurons in order to couple transcriptional network changes with

alterations in histone modifications resulting from ELE. We therefore crossed NuTRAP reporter [28] with Emx1- *Cre* [31, 32] mouse lines to generate Emx1- *Cre*; NuTRAP transgenic progeny for this study (Figure 1A). In the presence of a *loxP* site-flanked sequence, Emx1- *Cre* facilitates recombination in approximately 88% of neurons in the neocortex and hippocampus, and in less than 2% of GABAergic inhibitory interneurons in these regions [31]. Emx1- *Cre* also targets neural progenitor cells and can be expressed in mature astrocytes in striatum [33]. Of note, we exclusively used Emx1- *Cre* female mice in our breeding schemes given that the *Cre* -recombinase has been reported to be expressed in a subset of male germline cells [34].

We sought to validate neuron-specific expression of the NuTRAP cassette. First, immunohistochemistry of Emx1-NuTRAP hippocampal slices show distinct GFP and mCherry expression in CA1 and CA3 pyramidal neurons (Figure 1B-C) as well as the granule cell layer of the dentate gyrus (DG) (Figure 1D). Furthermore, mCherry positive nuclei remained intact and bound to the auto-fluorescent magnetic beads after our modified nuclear isolation procedure (Supplemental Figure 1A). As *Emx1*-expressing neural stem cells can become astrocytes [31], we sought to determine whether a significant number of mature astrocytes were obtained in the population of isolated cells. Flow cytometry experiments using THY-1 cell surface marker to label neurons and S100β as an astrocytic marker revealed a distinct population of cells double positive for GFP and THY-1, whereas a S100β and GFP double positive cell population was absent (Figure 1E).

To perform simultaneous isolation of labeled ribosomes and nuclei from the same homogenate, hippocampal tissue was dissected from both brain hemispheres, combined, and homogenized in one sample tube (Figure 1A). We then performed the INTACT and TRAP methods on isolated samples by starting the protocol with the beginning steps from the INTACT procedure, modified to include cycloheximide. Cycloheximide works rapidly to inhibit protein synthesis and is used for maintaining crosslinks between translating mRNA and ribosomal subunits during purification in the traditional TRAP method. Despite the presence of cycloheximide, nuclear morphology from *Emx1*-expressing neurons is overall unchanged

(Supplemental Figure 1A). Additionally, a Bioanalyzer was used to determine if there were cycloheximide-induced double-stranded DNA breaks in our nuclear preparation that could interfere with downstream DNA sequencing applications (such as ATAC, CUT&RUN, or CUT&Tag). We found no evidence of DNA double strand breaks generating fragments of less than 1kb (Supplemental Figure 2B). Following magnetic purification of biotin-labeled nuclei, the supernatant fraction was removed and taken through TRAP, while the pelleted nuclei were processed through the remaining steps of INTACT (see Methods). Combining bilateral hippocampi from a single mouse yielded TRAP-isolated RNA of high quality and sufficient concentration for sequencing (RIN > 8 for all samples, average yield RNA = 14.36688 ng/ul; Supplemental Table 1). INTACT-isolated nuclei were further processed using the CUT&RUN (Cleavage Under Targets and Release Using Nuclease[35]) method to isolate antibody-specific protein-DNA interactions for downstream DNA sequencing. The resulting DNA libraries were of high quality and concentration when using specific antibodies (H4K8ac: average size = 1197 bp, average concentration = 127.8 nM; H3K27me3: average size = 1056 bp, average concentration = 139.0 nM; Supplemental Table 1). In contrast, the resulting DNA libraries using the non-specific IgG control were of substantially lower concentrations (IgG: average size = 1075 bp, average concentration = 16.3 nM; Supplemental Table 1) further indicating that nuclear DNA from both isolations was of high starting quality.

In order to confirm our TRAP-isolated hippocampal mRNA came primarily from excitatory neurons, we took a bioinformatics approach to assess for neuronal gene enrichment. Specifically, we compared RNA-seq data from whole dorsal hippocampal tissue of wild-type mice to our TRAP-isolated RNA-seq data. We found that TRAP-isolated mRNA had significant enrichment of several neuronal genes including *Dlg4*, *Thy1*, *Eno2*, and *Syt4*, as well as a significant reduction in astrocytic, microglial, oligodendrocyte, and inhibitory neuron genes (Figure 1F). There was a relative expression increase of the glial fibrillary astrocytic protein (GFAP) in our TRAP samples. This gene can also be expressed in neural stem populations that were present in our whole hippocampus samples, so this finding may be a reflection

of the neural stem cell population of the dentate gyrus captured as part of our TRAP isolation [36, 37]. Overall, these findings suggest that the Emx1-NuTRAP mouse model is a valid tool for neuron-enriched isolation of sequencing-grade, translating mRNA and nuclear chromatin from the same cell homogenate.

Figure 1

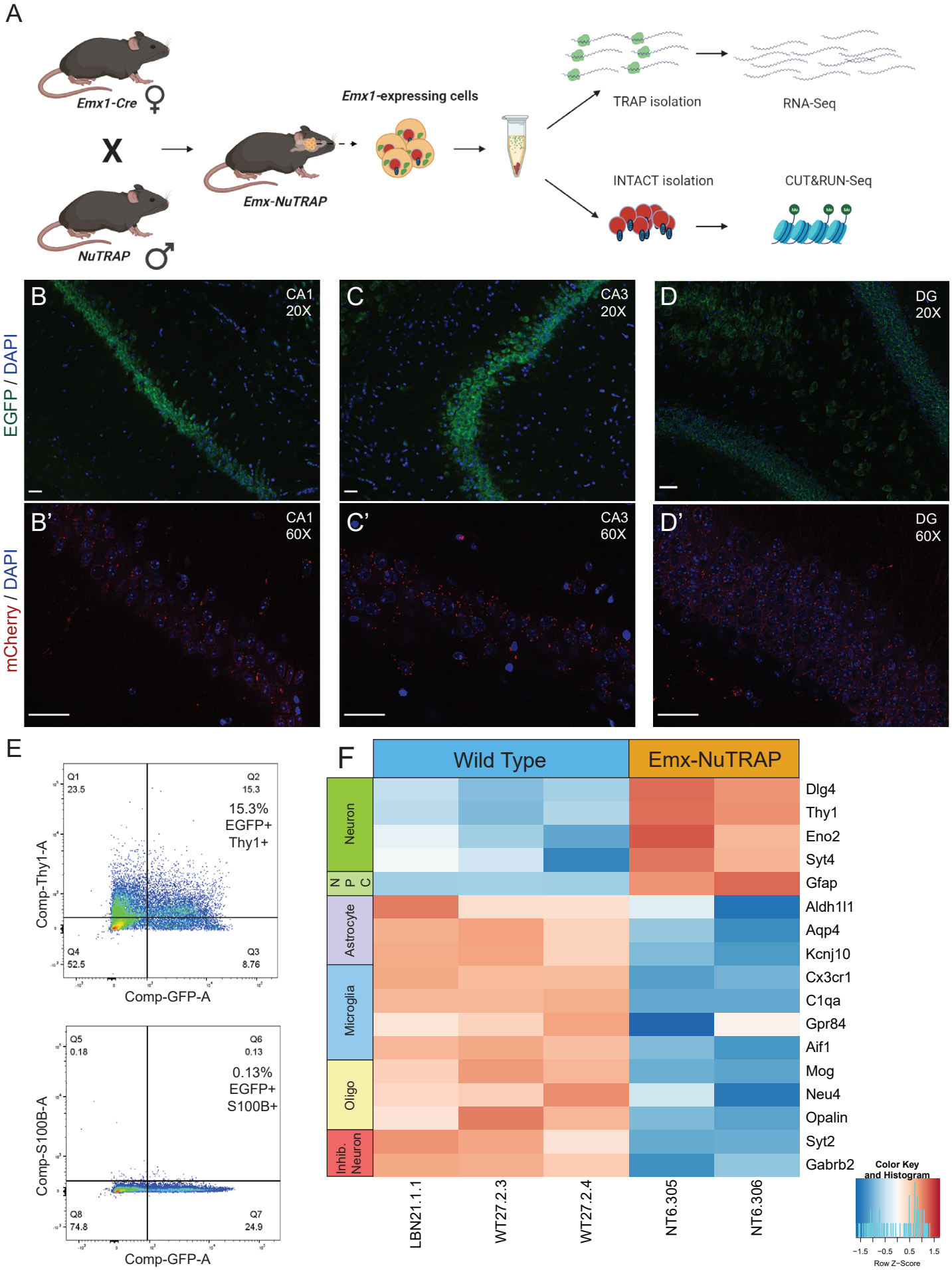
A
Emx1-Cre
X
NuTRAP
Emx-NuTRAP
Emx1-expressing cells
TRAP isolation
RNA-Seq
INTACT isolation
CUT&RUN-Seq
EGFP / DAPI
mCherry / DAPI
B
CA1
20X
C
CA3
20X
D
DG
20X
B'
CA1
60X
C'
CA3
60X
D'
DG
60X
E
Q1
23.5
Q2
15.3
15.3%
EGFP+
Thy1+
Q4
52.5
Q3
8.76
Comp-Thy1-A
Comp-GFP-A
Q5
0.18
Q6
0.13
0.13%
EGFP+
S100B+
Q8
74.8
Q7
24.9
Comp-S100B-A
Comp-GFP-A
F
Wild Type
Emx-NuTRAP
Neuron
N P C
Astrocyte
Microglia
Oligo
Inhib. Neuron
Dlg4
Thy1
Eno2
Syt4
Gfap
Aldh1l1
Aqp4
Kcnj10
Cx3cr1
C1qa
Gpr84
Aif1
Mog
Neu4
Opalin
Syt2
Gabrb2
LBN21.1.1
WT27.2.3
WT27.2.4
NT6.305
NT6.306
Color Key and Histogram
−1.5
−0.5
0.5
1.5
Row Z−Score

Figure 1. Generation and validation of the Emx1-NuTRAP mouse (A) Schematic representation of the Emx1-NuTRAP mouse generation and workflow of the simultaneous isolation protocol. (B) Immunofluorescence imaging of the CA1 region of the hippocampus at 20x objective (B) and 60x objective (B') after incubation with an mCherry antibody overnight. (C) Immunofluorescence imaging of the CA3 and CA2 region of the hippocampus at 20x objective (C) and 60x objective (C') after incubation with an mCherry antibody overnight. (D) Immunofluorescence imaging of the DG region of the hippocampus at 20x objective (D) and 60x objective (D') after incubation with an mCherry antibody overnight. Scale bars are set to 50µm for all images (B-D). (E) Flow cytometry for EGFP, THY-1, and S100β (15.3% of cells THY-1+/EGFP+ and 0.13% of cells S100β+/EGFP+). (F) Heatmap of differentially expressed neuronal and other cell type markers from RNA-seq data comparing TRAP isolated RNA from our Emx1-NuTRAP mice and previously generated dorsal hippocampal tissue RNA from wild type.

Performing INTACT/TRAP on the same or separate cell suspensions yields highly comparable RNA-seq and CUT&RUN-seq results.

Previous methods for performing INTACT and TRAP using NuTRAP mice have taken separate tissue homogenates for each procedure [28, 38]. In this study, we performed simultaneous isolation of nuclei and RNA from a single tissue homogenate containing bilateral hippocampi (referred to as "simultaneous isolations"). To determine if our approach of simultaneous INTACT and TRAP isolations does not interfere with data interpretation, we also performed separate INTACT and TRAP from hippocampal tissue obtained from one brain hemisphere for each method, counterbalancing for left versus right (we refer to this protocol as "separate isolations"). A Bioanalyzer was used to determine the amount and quality of the RNA obtained from each type of isolation (Separate isolations: average RNA concentration = 7.805 ng/ul, average RIN = 9.5; Simultaneous isolations: average RNA concentration = 14.367 ng/ul, average RIN = 9.3; Supplemental Table 1). The average RNA yield from the separate isolations (using a unilateral hippocampus) was approximately equal to half of the average yield of the simultaneous isolations (which combined bilateral hippocampi; Supplemental Table 1). Similarly, the final library concentrations for the separately isolated IgG CUT&RUN libraries were also approximately half the concentration of the simultaneous (Average simultaneous: 24.2nM, Average separate: 11nM; Supplemental Table 1). We interpret this to mean that nuclear DNA was fully intact in the simultaneous isolation because we did not obtain substantially more than double the concentration in the simultaneous vs separate isolations. Unilateral hippocampal homogenates yielded sufficient sequencing concentrations and quality to allow for library preparations from individual mice (Supplemental Table 1).

To determine if normalized RNA-seq counts were similar between the two isolation methods, we performed a Spearman's Rank-Order Correlation between the datasets from sedentary mice. The two RNA-seq datasets were found to be highly correlated, with R values greater than 0.5 and p value less than 2.2×10^{-16} ($R=1$, $p<2.2\times10^{-16}$; Figure 2A). CUT&RUN sequencing was used to identify genomic regions interacting with either H4K8ac, an activating histone post-translational modification

(PTM), or H3K27me3, a generally repressive histone PTM. We again applied Spearman's Rank-Order Correlation to understand whether the simultaneous vs separate INTACT isolation methods could influence CUT&RUN peak distribution. We compared normalized count data for CUT&RUN peaks across a representative chromosome (chromosome 2). We binned 100bp increments along the entire chromosome from the simultaneous and separate isolations using datasets generated from sedentary mice. Normalized sequencing counts, which reflected reads assigned to binned genomic regions along chromosome 2, were highly similar between conditions (H4K8ac: $R=0.65$, $p<2.2x10^{-16}$, H3K27me3: $R=0.81$, $p<2.2x10^{-16}$; Figure 2B-C). Taken together, these experiments suggest that translating mRNA and nuclear DNA isolated from hippocampal homogenates using either simultaneous or separate isolation procedures are comparable in terms of quality, concentration, functional characterization, and normalized sequencing reads.

We next wanted to determine if the different isolation methods could bias resulting gene expression on the basis of gene length. When plotting gene length against log fold change of gene expression, we see a similar distribution pattern of ELE-induced differentially expressed hippocampal genes (DEGs) between the simultaneous and separate methods (Figure 2D-E). We then compared the ELE-induced DEGs obtained using either the separate or the simultaneous isolation methods. Although many of the genes did not overlap (Figure 2F-G), most Gene Ontology (GO) terms did (14/20 GO terms for upregulated genes and 15/17 for downregulated genes; Figure 2H-K, Supplemental Table 2).

Figure 2

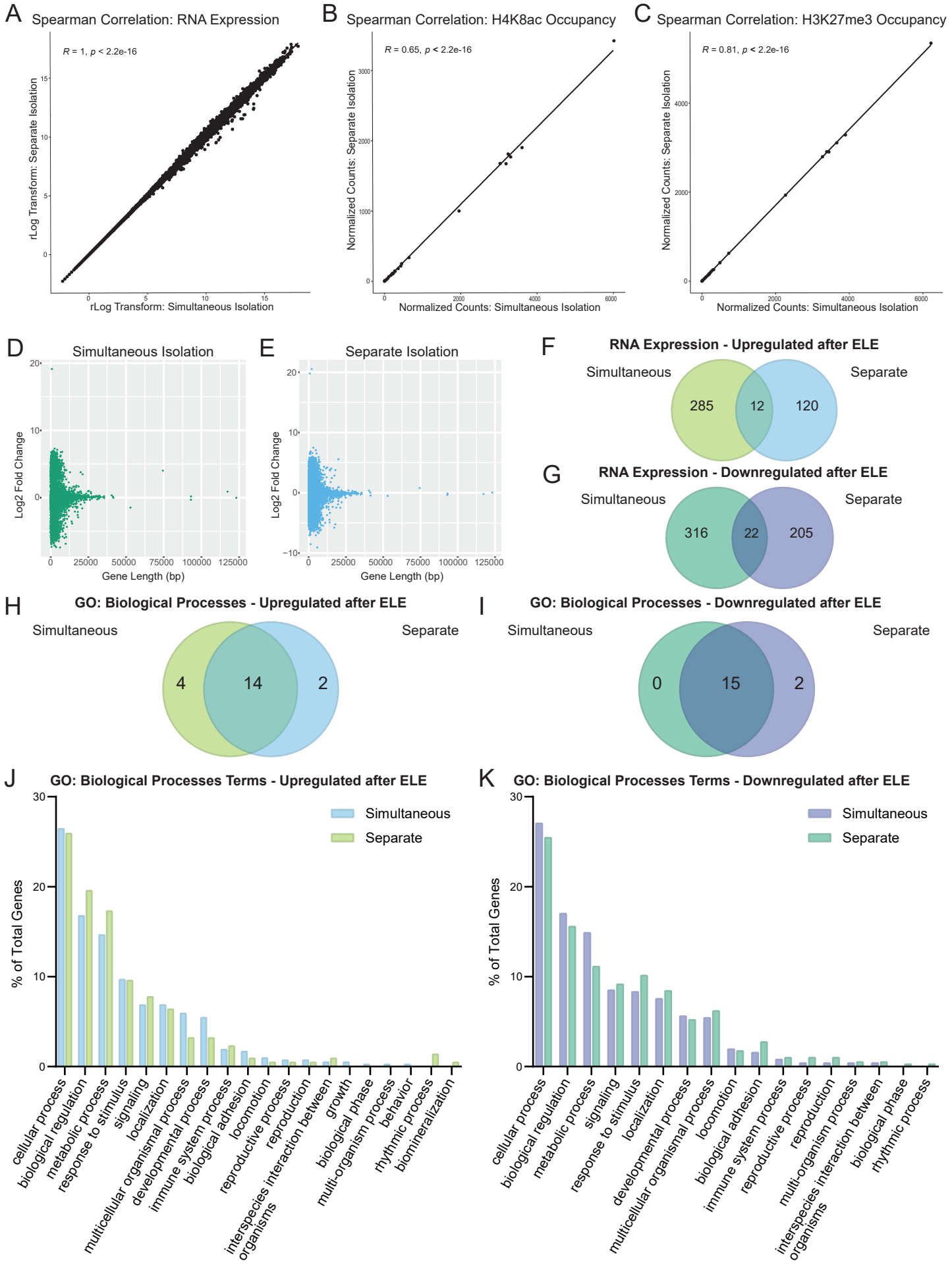
A
Spearman Correlation: RNA Expression
R = 1, p < 2.2e-16
rLog Transform: Separate Isolation
rLog Transform: Simultaneous Isolation
B
Spearman Correlation: H4K8ac Occupancy
R = 0.65, p < 2.2e-16
Normalized Counts: Separate Isolation
Normalized Counts: Simultaneous Isolation
C
Spearman Correlation: H3K27me3 Occupancy
R = 0.81, p < 2.2e-16
Normalized Counts: Separate Isolation
Normalized Counts: Simultaneous Isolation
D
Simultaneous Isolation
Log2 Fold Change
Gene Length (bp)
E
Separate Isolation
Log2 Fold Change
Gene Length (bp)
F
RNA Expression - Upregulated after ELE
Simultaneous
Separate
285
12
120
G
RNA Expression - Downregulated after ELE
Simultaneous
Separate
316
22
205
H
GO: Biological Processes - Upregulated after ELE
Simultaneous
Separate
4
14
2
I
GO: Biological Processes - Downregulated after ELE
Simultaneous
Separate
0
15
2
J
GO: Biological Processes Terms - Upregulated after ELE
Simultaneous
Separate
% of Total Genes
cellular process
biological regulation
metabolic process
response to stimulus
signaling
localization
multicellular organismal process
developmental process
immune system process
biological adhesion
locomotion
reproductive process
reproduction
interspecies interaction between organisms
growth
biological phase
multi-organism process
behavior
rhythmic process
biomineralization
K
GO: Biological Processes Terms - Downregulated after ELE
Simultaneous
Separate
% of Total Genes
cellular process
biological regulation
metabolic process
signaling
response to stimulus
localization
developmental process
multicellular organismal process
locomotion
biological adhesion
immune system process
reproductive process
reproduction
multi-organism process
interspecies interaction between organisms
biological phase
rhythmic process

Figure 2. Simultaneous and separate isolations of DNA and RNA from Emx1-NuTRAP mice are comparable. (A) Spearman Correlation for RNA expression between separately isolated RNA and simultaneously isolated RNA (n=2 mice for simultaneous isolations and 3 mice for separate isolations for Figures 2A-E, R=1, $p<2.2x10^{-16}$). (B) Spearman correlation between separate and simultaneously isolated DNA from CUT&RUN-seq for H4K8ac with 100bp chromosome 2 position bins (R=0.65, $p<2.2x10^{-16}$). (C) Spearman correlation between separate and simultaneously isolated DNA from CUT&RUN-seq for H3K27me3 with 100bp chromosome 2 position bins (R=0.81, $p<2.2x10^{-16}$). (D) Gene length versus fold change distribution plot for simultaneously isolated RNA. (E) Gene length versus fold change distribution plot for separately isolated RNA. (F) Genes upregulated in Emx1-NuTRAP RNA-seq after ELE in either simultaneous (n=2 sedentary mice and n=3 ELE mice) or separate isolations (n=3 mice per group). (G) Genes downregulated in Emx1-NuTRAP RNA-seq after ELE in either simultaneous or separate isolations. (H, I) Panther Gene Ontology: Biological Processes Venn diagram (H) and bar graph of gene distributions (I) for genes upregulated after ELE in either separate or simultaneous isolations. (J, K) Panther Gene Ontology: Biological Processes Venn diagram (J) and bar graph of gene distributions (K) for genes downregulated after ELE in either separate or simultaneous isolations.

Early-life exercise promotes expression of plasticity-related genes and is associated with transcriptional regulatory pathways implicated in hippocampal memory.

To identify the transcriptional effects of ELE in hippocampal neurons, we performed cell-type specific bulk sequencing on RNA extracted from Emx1-NuTRAP hippocampi using the simultaneous isolation approach. We compared DEGs from sedentary mice vs mice that underwent voluntary wheel running between postnatal days (p) 21-41. Using DESeq2 to assess for DEGs (>30% expression increase with a p value < 0.05) we found that voluntary exercise during juvenile-adolescence significantly alters gene expression in *Emx1* expressing neurons (297 upregulated and 338 downregulated genes; Figure 3A and Supplemental Table 2). Many of the genes upregulated after ELE are also known to be involved in exercise or hippocampal memory mechanisms, including BDNF [39] and NR4A1 [40]. To functionally categorize ELE-induced DEGs, we performed a Panther Gene Ontology (GO) analysis [41] focusing on the Molecular Function categorization and separated by upregulated and downregulated genes. The GO term categories with the most genes functionally assigned to them were binding, catalytic activity, molecular function regulator, transporter activity, molecular transducer activity, and structural molecule activity (Figure 3B). Many of the genes driving these results are known to be important in neuronal function (*Kcna1, Slc24a4, Stxbp5l, Gabra2,* and *Camk2n2*), neurodevelopment (*Artn, Kdm7a, Sox21, Gap43,* and *Efna5*), and hippocampal memory (*Bdnf, Nr4a1* and *Dusp5*).

To evaluate possible transcription factors and upstream regulators implicated by ELE-induced DEGs, we applied Qiagen's Ingenuity Pathway Analysis (IPA) to our RNA-seq dataset [42]. The top six upstream regulators by significance included CREB1, KMT2A, LEF1, SMAD3, EGR1, and MITF. Each of the top five transcription factors have been implicated in hippocampal development or function (Figure 3C and Supplemental Table 3) [43-50]. The transcription factors KMT2A and LEF1 have not been previously associated with the effects of exercise on hippocampal function. Interestingly, both CREB1 and KMT2A have histone modifying properties; CREB1 through its associated CBP [51] and KMT2A through its methyltransferase activity

[44]. LEF1 has been shown to regulate neural precursor proliferation in the hippocampus [45]. SMAD3 is critical for intermediate progenitor cell survival and negatively regulates serum insulin after exercise [46, 47]. EGR1 is an immediate early gene that recruits TET1 DNA demethylase during neural activation and development [48]. MITF was the sixth upstream regulator identified and is a transcription factor linked to autophagy mechanisms [49]. These specific transcription factors were not significantly differentially expressed in our RNA-seq dataset; however, their activity may not be linked to a change in their own expression after ELE but rather is modulated by exercise to influence programs of gene expression.

To further understand whether the transcriptional profiles resulting from ELE were enriched for specific, *a priori* assigned molecular functions, we performed Gene Set Enrichment Analysis (GSEA) [52]. We evaluated the "Reactome" category of functional gene sets followed by a leading edge analysis to further determine which genes were driving the significant categories (Figure 3D and Supplemental Table 4). Of the DEGs upregulated after ELE, several interesting categorizations and the genes driving them were revealed. The genes *H3c4*, *H2bc3*, *H2bc5*, and *H2bc9* genes, which encode histone family member proteins, were driving the categories DNA methylation, HDACs deacetylate histones, and transcriptional regulation by smRNAs. Meiosis and meiotic recombination also emerged in these results which was unusual; however, leading edge analysis showed many of these genes (*Atm, Blm, Msh4*, and *Mnd1*) to be generally involved in cell-cycling processes. Exercise is well known to increase adult neurogenesis in hippocampal dentate gyrus and can explain cell cycle gene enrichment in our dataset [16]. Several nucleoporin complex genes (*Nup35/ 42/ 43/ 50/ 58/ 62/ 93/ 107/ 153/ 210*) were also identified for their associations with categories such as: gene silencing by RNA, nuclear envelope breakdown, transport of mature mRNAs derived from intronless transcripts. *Nup* genes form a variety of nuclear pore complexes that play critical roles in cellular processes including cell-cycle regulation, cellular differentiation, and epigenetic control [53].

Of the downregulated pathways identified, translation-associated categories (translation, eukaryotic translation initiation/elongation, and SRP-dependent co-translational protein targeting to membrane) were driven by significant downregulation of ribosomal protein gene families (*Rps*, *Rpl*, *Rplp*) and eukaryotic initiation factor 3 (*eIF3*) subunits. Over-expression of *eIF3* subunits has been linked to Parkinson's Disease and altered expression of *eIF3* has been associated with neurodevelopmental disorders [54]. Additionally, collagen genes (*Col1a1*, *Col1a2*, *Col2a1*, *Col3a1*, and *Col5a1*) were downregulated after ELE, leading to the identification of categories including: MET activates PTK2 signaling, MET promotes cell motility, and collagen degradation. *Col1a1* and *Col1a2* have been previously identified as putative aging genes that decrease in their expression after chronic exercise in adults [55]. By analyzing these enriched pathways and the networks of genes driving them, we were able to identify a number of transcriptional programs activated by ELE that could be candidates for further exploration.

Figure 3

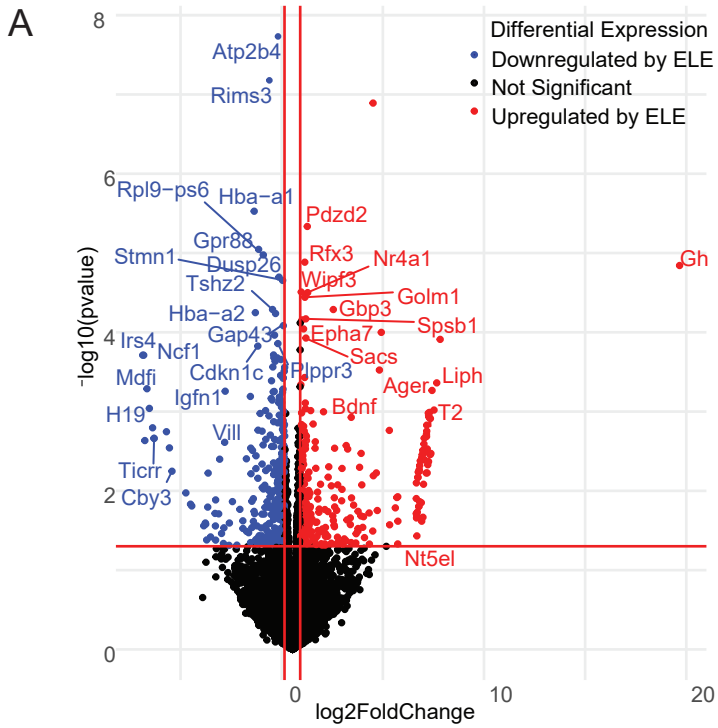

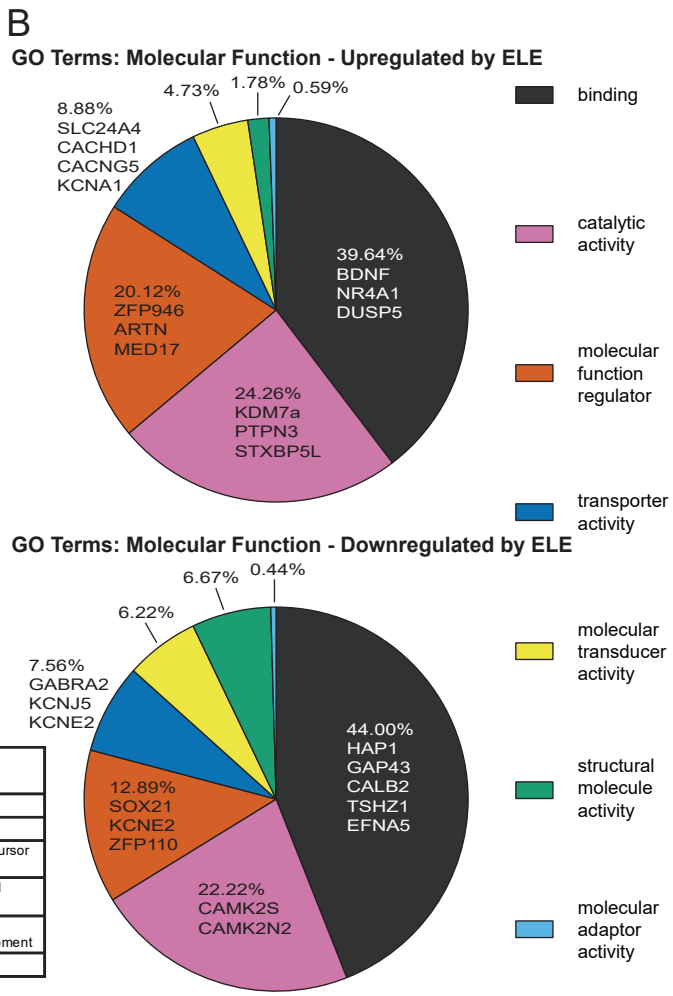

C

Predicted Activated Upstream Regulator	p-value of overlap	# Target Molecules in Dataset	Function
CREB1	1.11E-03	14	Transcription factor required for LTM
KMT2A	1.90E-03	5	Lysine methyltransferase active in development
LEF1	4.12E-03	6	Transcription factor that may regulate neural precursor cell proliferation in the hippocampus
SMAD3	1.80E-02	7	Critical for intermediate progenitor cell survival and negatively regulates serum Irisin after exercise
EGR1	3.52E-02	5	Immediate early gene that recruits TET1DNA demethylase during neural activation and development
MITF	3.58E-02	6	Transcription factor import for autophagy

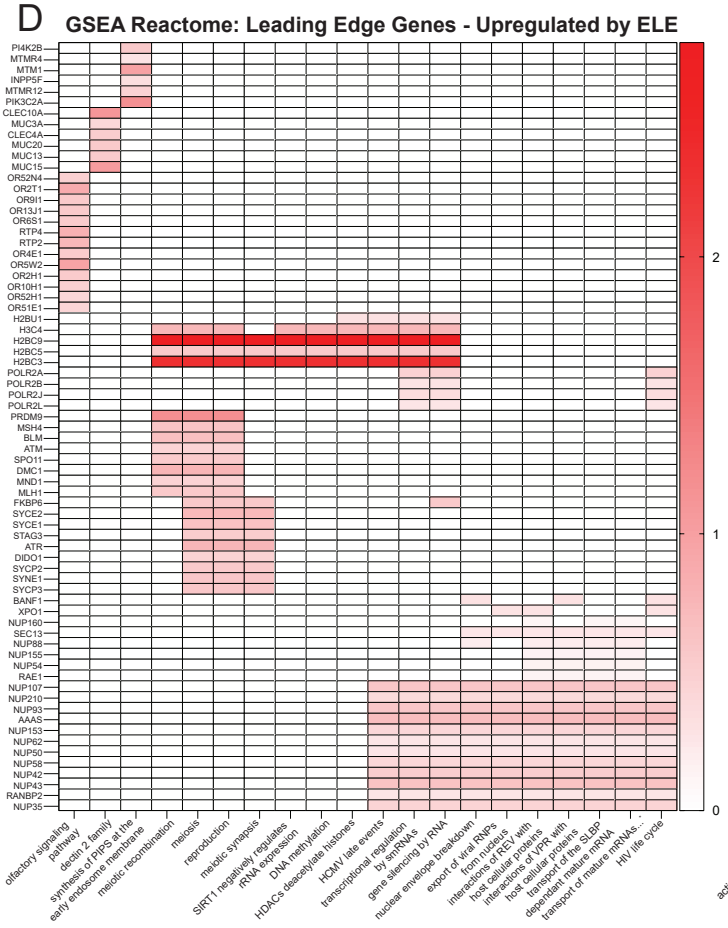

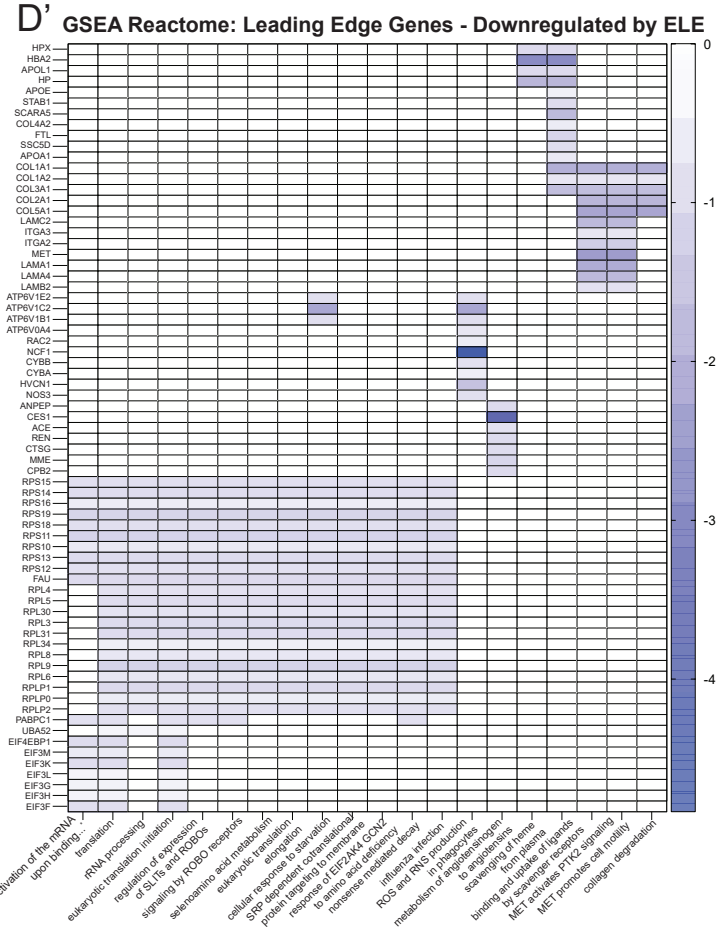

Figure 3: ELE leads to transcriptomic changes in hippocampal neurons during adolescence. (A) Volcano plot of significantly differentially expressed genes from RNA-seq on ELE versus sedentary samples (n=2 sedentary mice and n=3 ELE mice, absolute value $\log_2$ fold change > 0.3785 and p-value < 0.05). (B) Panther Gene Ontology: Molecular Function top terms by most genes assigned. (C) Top 6 upstream regulators identified by Ingenuity Pathway Analysis (IPA). (D) Representative Gene Set Enrichment Analysis: Reactome leading edge diagrams showing genes that are upregulated (D) or downregulated (D') in ELE, and their enrichment. *Abbreviated terms in (D) transport of mature mRNAs derived from intronless transcripts, (D') activation of the mRNA upon binding of the cap binding complex and EIFs and subsequent binding to 43S.

Neuronal H4K8ac is enriched and H3K27me3 is reduced at a subset of plasticity genes after early-life exercise.

The power of the Emx1-NuTRAP mouse model coupled with the simultaneous isolation procedure is the ability to directly correlate differential gene expression with candidate epigenetic mechanisms in the same cells. Hippocampal nuclei were obtained using INTACT methods in our simultaneous isolation procedure, followed by CUT&RUN-seq from nuclear chromatin. We investigated ELE-induced changes in histone modifications H3K27me3 and H4K8ac across the genome. H4K8ac is a permissive histone modification that has been shown to be enriched at *Bdnf* and its presence correlates improved hippocampal memory after exercise [22]. H3K27me3 is a repressive histone mark and a common control in CUT&RUN studies [35, 56] and is decreased at the *Bdnf* promoter region after conditional fear context training [57]. Peaks were called using SEACR [58] and histone modification enrichment peaks were overlapped with differentially expressed genes (Figure 4A). We correlated H4K8ac and H3K27me3 peaks present with upregulated and downregulated RNA as a result of ELE. The loss of either H3K27me3 or H4K8ac as a result of ELE did not correlate with changes in RNA expression. This may indicate that ELE-induced additions of these two histone modification, but not their removal, underlie differential gene expression. 93 upregulated genes correlate with new H4K8ac peaks while 33 downregulated genes correlate with new H3K27me3 peaks (Figure 4B and Supplemental Table 5). However, loss of only one H4K8ac peak correlates with downregulation of RNA, and loss of only two H3k27me3 peaks correlate with upregulation of RNA (Figure 4B and Supplemental Table 5). Unsurprisingly, many of the peaks we discovered newly present as a result of ELE did not correlate with expression changes in a large number of genes. Notable upregulated genes with new H4K8ac after ELE are *Prox1*, *Sntb2*, and *Kptn*. PROX1 is involved governing differentiation, maturation, and DG versus CA3 cell identity in intermediate progenitor cells of the hippocampal DG [59], while SNTB2 is involved in G protein-coupled receptor cell signaling [60]. KPTN encodes a protein involved in cytoskeletal cell structure, and its mutation can cause neurodevelopmental disability and seizures [61]. Interestingly, downregulated

genes found to have new H3K27me3 after ELE included *Col3a1*, *Efnb2*, *Epop*, and *Myoc*. COL3A1 and MYOC are structural proteins involved in the extracellular matrix and the cytoskeleton respectively [62-64]. EFNB2 is a signaling molecule involved in cell migration and its haploinsufficiency can cause neurodevelopmental disability [65-67]. EPOP is a known editor of the chromatin landscape by altering H2Bub and H3K4me3 distributions [68, 69]. Interestingly, many of the histone modification changes that occurred as a result of exercise appear to be in distal intergenic regions for H3K27me3 and intronic regions for H4K8ac (Figure 4C). To investigate how ELE-induced changes to histone PTM distribution might alter gene expression, we looked at the distribution of peaks around one representative gene of interest increased after ELE: *Prox1* (Figure 4D). Taken together, these results suggest that ELE promotes the new addition of H4K8ac and H3K27me3 PTMs to regulate gene expression. Given that the majority of identified peaks did not correlate with DEGs, they may instead implicate regions of interest that are "primed" for facilitated gene expression following future stimuli, such as learning.

Figure 4

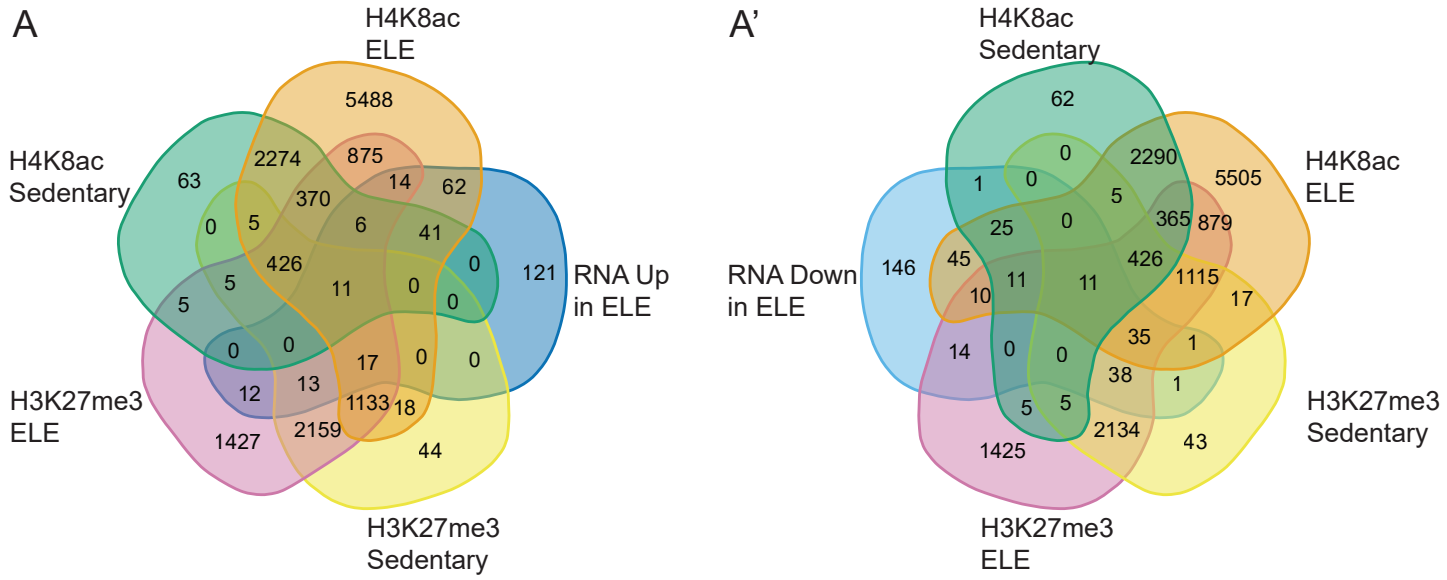
A
H4K8ac ELE
H4K8ac Sedentary
RNA Up in ELE
H3K27me3 ELE
H3K27me3 Sedentary
5488
875
2274
63
370
14
62
0
5
6
41
426
0
121
5
11
0
0
0
0
17
0
0
12
13
1133
18
1427
2159
44
A'
H4K8ac Sedentary
H4K8ac ELE
RNA Down in ELE
H3K27me3 Sedentary
H3K27me3 ELE
62
0
2290
5505
1
0
5
25
0
365
879
146
45
426
1115
10
11
11
17
35
1
14
0
0
38
1
5
5
2134
43
1425

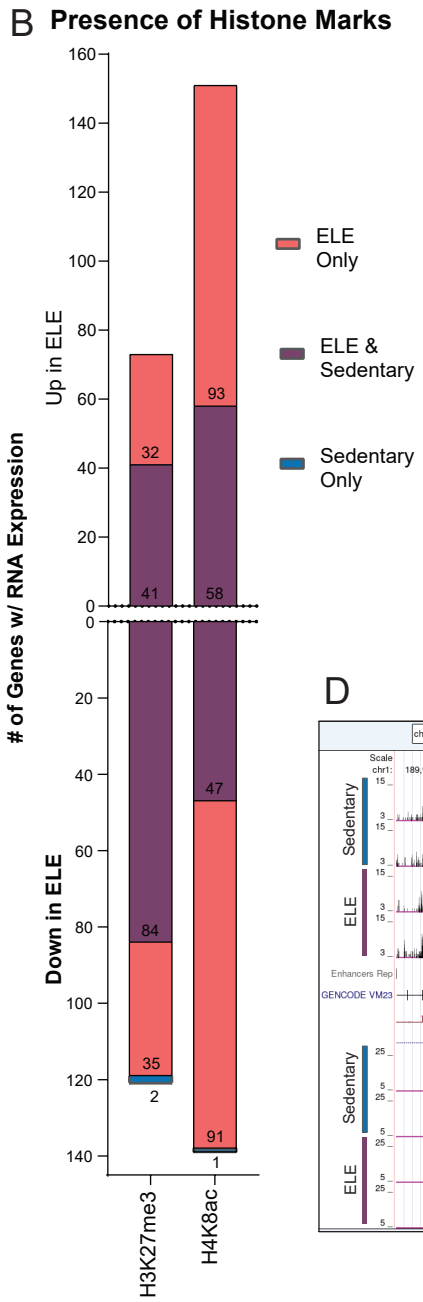
B Presence of Histone Marks
# of Genes w/ RNA Expression
Up in ELE
Down in ELE
ELE Only
ELE & Sedentary
Sedentary Only
H3K27me3
H4K8ac
32
41
93
58
84
35
2
47
91
1

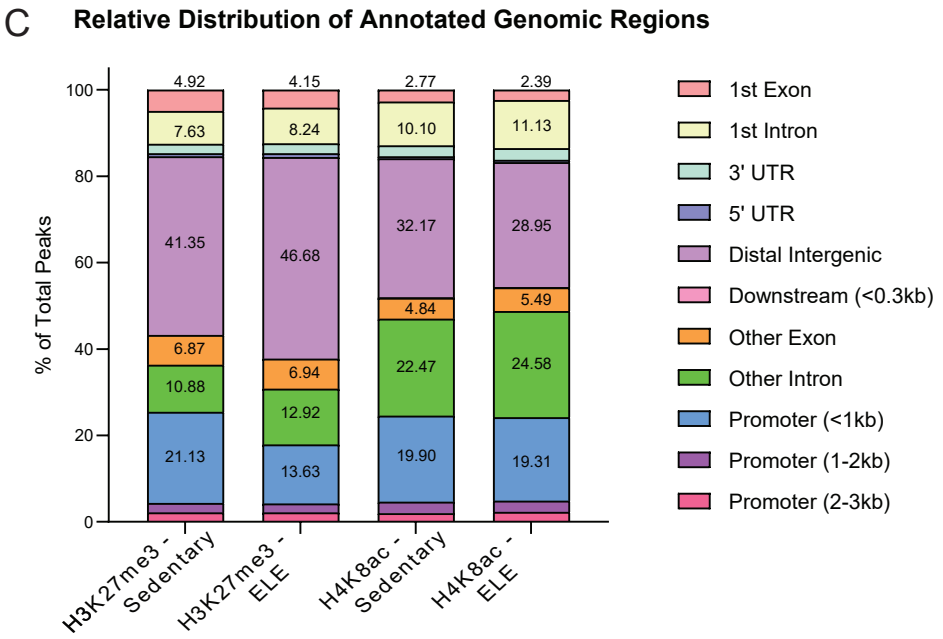
C Relative Distribution of Annotated Genomic Regions
% of Total Peaks
H3K27me3 - Sedentary
H3K27me3 - ELE
H4K8ac - Sedentary
H4K8ac - ELE
4.92
4.15
2.77
2.39
7.63
8.24
10.10
11.13
41.35
46.68
32.17
28.95
6.87
6.94
4.84
5.49
10.88
12.92
22.47
24.58
21.13
13.63
19.90
19.31
1st Exon
1st Intron
3' UTR
5' UTR
Distal Intergenic
Downstream (<0.3kb)
Other Exon
Other Intron
Promoter (<1kb)
Promoter (1-2kb)
Promoter (2-3kb)

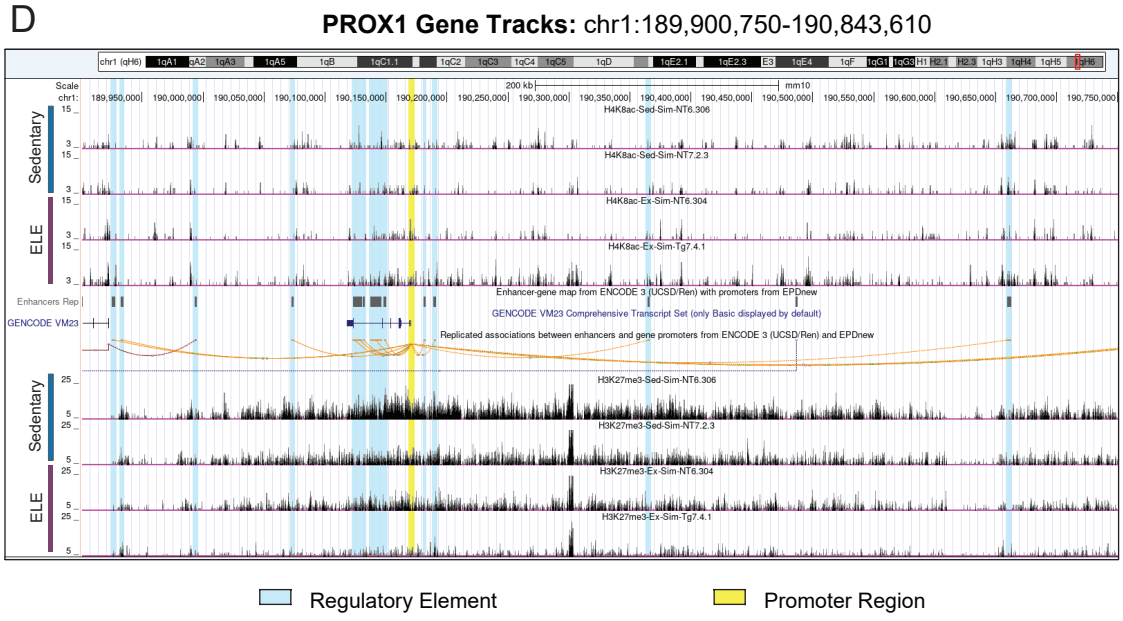
D
PROX1 Gene Tracks: chr1:189,900,750-190,843,610
Sedentary
ELE
Enhancers Rep
GENCODE VM23
Regulatory Element
Promoter Region

Figure 4: ELE alters H4K8ac and H3K27me3 occupancy. (A) Venn diagram of gene peaks identified in CUT&RUN for H4K8ac and H3K27me3 by SEACR (top 1% of peaks FDR<0.1) overlapped with genes upregulated (A) and downregulated (A') in RNA by ELE (n=2 sedentary mice and n=3 ELE mice). (B) CUT&RUN SEACR peak calls at genes that overlap with genes differentially expressed by ELE as determined by RNA-seq. (C) Stacked bar of the relative distribution of peak calls at various genomic regions identified by CUT&RUN called using SEACR. (D) Representative track of CUT&RUN data around *Prox1* showing differential peak height between ELE and sedentary conditions for H4K8ac and H3K27me3.

Neuron-specific gene expression and histone PTMs are functionally comparable between left and right hippocampal hemispheres.

Many studies take advantage of the brain's structural symmetry by using tissue from each hemisphere for separate molecular processing. Prior evidence that hippocampal lateralization can influence LTP, hemisphere-specific glutamate receptor density, and performance in certain memory tasks [70]. We wanted to determine if there were differences in transcriptional programs resulting from ELE in left vs right hippocampi. Using the separate isolation approach described above, we compared the differential gene expression as a result of ELE between left and right hemispheres. We found that although individual gene expression patterns were different between left and right hippocampal hemispheres (Figure 5A-B), the Panther GO: Biological Processes terms were substantially similar with most categories overlapping (Figure 5C-F). This could suggest spatial or hemispheric assignment of genes with functional similarity.

Finally, we wanted to determine if left and right hippocampal hemispheres had significant differences in DEGs and CUT&RUN sequencing peak distributions at baseline (without exercise). We performed Spearman's Rank-Order Correlation on the transcript counts from the RNA-seq ($R=1$, $p<2.2\times10^{-16}$; Figure 5G), and the CUT&RUN 100 bp binned peak counts for H3K27me3 ($R=0.70$, $p<2.2\times10^{-16}$; Figure 5H) and for H4K8ac ($R=0.59$, $p<2.2\times10^{-16}$; Figure 5I). We found that the seq peaks and transcript counts were very similar with significance considered as R values greater than 0.5 and p value less than 2.2×10^{-16} (Figure 5G-I). These data suggest that in the sedentary condition, left and right hippocampal hemispheres yield similar normalized sequencing counts.

Figure 5

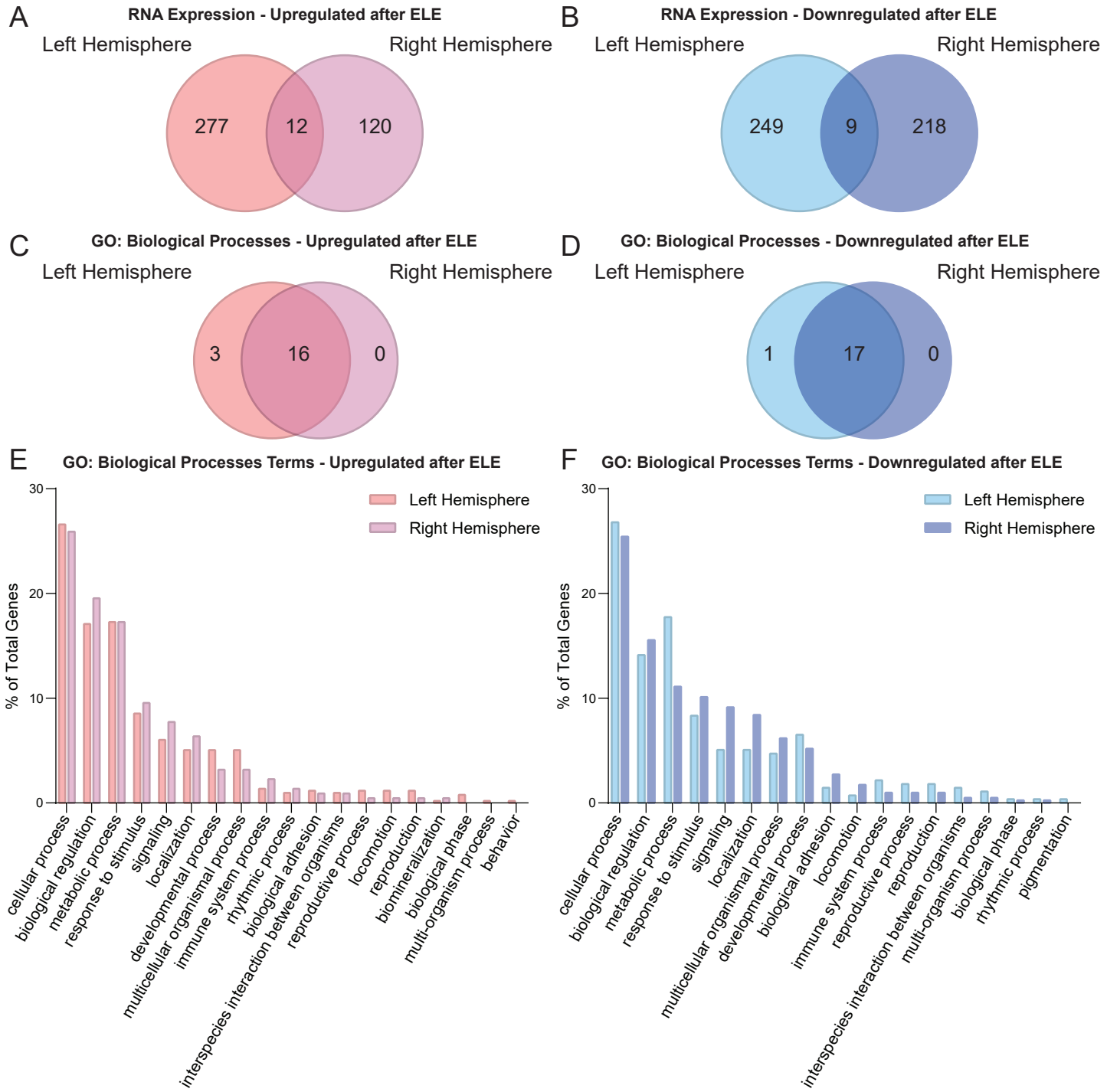
A
RNA Expression - Upregulated after ELE
Left Hemisphere
Right Hemisphere
277
12
120
B
RNA Expression - Downregulated after ELE
Left Hemisphere
Right Hemisphere
249
9
218
C
GO: Biological Processes - Upregulated after ELE
Left Hemisphere
Right Hemisphere
3
16
0
D
GO: Biological Processes - Downregulated after ELE
Left Hemisphere
Right Hemisphere
1
17
0
E
GO: Biological Processes Terms - Upregulated after ELE
Left Hemisphere
Right Hemisphere
% of Total Genes
0
10
20
30
cellular process
biological regulation
metabolic process
response to stimulus
signaling
localization
developmental process
multicellular organismal process
immune system process
rhythmic process
biological adhesion
interspecies interaction between organisms
reproductive process
locomotion
reproduction
biomineralization
biological phase
multi-organism process
behavior
F
GO: Biological Processes Terms - Downregulated after ELE
Left Hemisphere
Right Hemisphere
% of Total Genes
0
10
20
30
cellular process
biological regulation
metabolic process
response to stimulus
signaling
localization
multicellular organismal process
developmental process
biological adhesion
locomotion
immune system process
reproductive process
reproduction
interspecies interaction between organisms
multi-organism process
biological phase
rhythmic process
pigmentation
G
Spearman Correlation: RNA Expression
R = 1, p < 2.2e−16
rLog Transform: Left Hemisphere
rLog Transform: Right Hemisphere
H
Spearman Correlation: H4K8ac Occupancy
R = 0.59, p < 2.2e-16
Normalized Counts: Left Hemisphere
Normalized Counts: Right Hemisphere
I
Spearman Correlation: H3K27me3 Occupancy
R = 0.7, p < 2.2e-16
Normalized Counts: Left Hemisphere
Normalized Counts: Right Hemisphere

Figure 5: Histone modifications and functional categorizations of gene expression are similar regardless of hemispheric origin of hippocampal tissue. (A-B) Venn diagram of genes upregulated (A) or downregulated (B) by ELE identified between the left and right hemispheres by the separate isolation protocol RNA-seq (n=3 mice per group). (C-D) Venn diagram of Panther Gene Ontology: Biological Process terms for genes upregulated (C) or downregulated (D) by ELE identified between the left and right hemispheres by the separate isolation protocol RNA-seq. (E-F) Percent of genes fitting into each GO category for the left and right hemisphere for genes upregulated (E) and downregulated (F) by ELE by separate isolation RNA-seq. (G) Spearman correlation between the left and right hemispheres RNA-seq data from the separate isolation protocol of sedentary rlog normalized expression ($R=1$, $p<2.2x10^{-16}$). (H) Spearman correlation between hemispheres for CUT&RUN H4K8ac normalized count data for chromosome 2 in 100bp bins ($R=0.59$, $p<2.2x10^{-16}$). (I) Spearman correlation between hemispheres for CUT&RUN H3K27me3 normalized count data for chromosome 2 in 100bp bins ($R=0.7$, $p<2.2x10^{-16}$).

Discussion

Here we present results demonstrating cell-type specific, simultaneous characterization of translating mRNA and associated histone modifications from a single population of hippocampal neurons obtained from ELE mice. To our knowledge this is the first report describing use of the NuTRAP construct in a predominantly neuronal population. Additionally, our unique experimental approach is a technical advance for NuTRAP applications: by modifying the nuclear chromatin isolation (INTACT) procedure to include cycloheximide, one can obtain both polyribosome-bound mRNA (using TRAP) and nuclear DNA from a single lysate to directly correlate gene expression programs with epigenetic regulatory mechanisms in the same set of cells. The field of neuroepigenetics has been challenged by very limited approaches for coupling cell-type specific transcriptional profiles with chromatin modifications without compromising cell integrity (through flow sorting) or genomic coverage (through single-cell sequencing). Therefore, the NuTRAP model offers an exciting opportunity to overcome these challenges and perform paired transcriptomic and epigenomic analyses in any cell type of interest for which a *Cre*-line exists.

Our study focuses on the impact of exercise on hippocampal gene expression and associated epigenetic modifications specifically during juvenile – adolescent periods (the fourth through sixth postnatal weeks of life in mice). We discover gene expression programs, and alterations in the histone modifications H4K8ac and H3K27me3, that may be unique to this early-life period. There have been recently published reports investigating the effects of voluntary exercise on adolescent and adult hippocampal gene expression and epigenetic modifications through RNA and DNA sequencing methods, however these used heterogenous cell populations [19, 20]. In our study, several genes with either chromatin-modifying or neurogenesis-regulating properties that were either upregulated with new H4K8ac (*Prox1*, *Sntb2*, and *Kptn*), or downregulated with new H3K27me3 (*Col3a1*, *Efnb2*, *Epop*, and *Myoc*). For example, ELE could promote the expression of *Prox1* by the addition of H4K8ac, and in turn, *Prox1* can promote neurogenic fate and cell location assignment (such as DG granule cell fate over CA3 pyramidal cell identity [71]). ELE was also found to

alter the expression of *Kptn,* a gene encoding a protein involved in actin dynamics and neuromorphogenesis. Increased *Kptn* expression and accessibility may possibly facilitate cytoskeletal changes occurring with altered synaptic plasticity after exercise. Overall, the differentially expressed genes and their associated chromatin states identified in this study provide molecular candidates involved in the effects of ELE on hippocampal function.

Traditional epigenetic and gene expression analyses of bulk hippocampal tissue are confounded by the cellular heterogeneity of the samples. Further, current methods for paired analysis of the epigenome and transcriptome are restricted by the need for multiple transgenic animal models or the use of highly expensive single-cell sequencing technologies. However, it is critical to obtain epigenomic information in a cell-type specific manner because there are unique epigenetic modifications distinguishing cell subtypes of the central nervous system (CNS) [10, 72]. Roh et al. first developed the NuTRAP mouse to characterize adipocyte-specific and hepatocyte-specific epigenetic and transcriptional profiles [29]. The NuTRAP mouse has since been used to perform paired transcriptome and DNA modification analysis in astrocytes and microglia, demonstrating its utility in CNS cell-types [38]. The Emx1-NuTRAP mouse described here provides rapid, cost-effective characterization of neuron-specific changes to epigenetic state and gene expression using whole-tissue homogenates with heterogeneous cell types. In our technical validation experiments, the combined INTACT and TRAP isolation procedures (simultaneous isolation) produced high quality RNA and DNA of sufficient concentration for downstream sequencing studies from a single mouse hippocampus. This method effectively increases the total sample size used for each analysis as the tissue sample does not need to be separated for DNA and RNA isolation. CUT&RUN and CUT&Tag allow for low-input cell-specific chromatin analysis [58, 73] further reducing the required amount of starting material. Indeed, the DNA obtained from the simultaneous INTACT and TRAP isolations could be used for other applications for evaluating the chromatin landscape, including ATAC-seq.

A common approach to paired transcriptomic and epigenomic analyses is to use separate brain tissue from one hemisphere for gene expression studies and the

other side for epigenetic analyses [74]. A previous study utilizing the NuTRAP allele in non-neuronal brain cells used separate brain hemispheres to perform INTACT and TRAP [75]. However, this assumes that cells of the same type from each half of the tissue will show the same epigenetic and transcriptional profile. This is not necessarily the case for all cell types, especially in the CNS, as structures of the brain can show high degrees of hemispheric specialization [76-80]. To address the degree of transcriptional or epigenetic difference between hippocampi from opposite hemispheres, we performed separate INTACT and TRAP isolations using hippocampal tissue from one hemisphere for DNA isolation and the contralateral hippocampus for mRNA isolation. We found that although differential gene expression and histone modifications differed between left and right hippocampi, functional analysis using gene ontology revealed similar biological processes between the two sides.

In summary, our work reveals ELE-induced transcriptomic and epigenomic signatures in hippocampal neurons using the Emx1-NuTRAP mouse we developed for such comparisons. Presently, the field is shifting to single-cell resolution for sequencing studies, however our study was performed in bulk tissue enriched for neurons. As the goal of this work was to characterize the transcriptional and epigenomic effects of early life exercise, cell subtype identity (as is often a priority in single-cell approaches) was not necessary to address this study's questions. Furthermore, single-cell approaches bias against lowly-expressed genes, which presents the risk of not capturing small expression changes in rate-limiting genes that may have large changes in function as a result of ELE. A limiting factor for the use of the NuTRAP transgenic mouse is the requirement of a Cre-line to exist for the experimenter's cell type of interest. In our Emx1-NuTRAP model the the Cre-recombinase in *Emx1* expressing cells is constitutively expressed, and this may present off-target effects when present during development. Despite this, our study uses a feasible, previously undescribed approach in the field of neuroepigenetics to pair transcriptomic and epigenomic bulk sequencing results from a population of hippocampal neurons, revealing new molecular epigenetic candidates for further

mechanistic studies to examine the effects of early life exercise on hippocampal function.

Methods

Resource Availability

Lead Contact

Further information and requests for resources and reagents should be directed to and will be fulfilled by the lead contact, Dr. Autumn Ivy (aivy@uci.edu)

Materials Availability

- No new reagents or materials were generated for this study.
- The mouse lines used for this study are available from Jackson Labs (Emx1-IRES-*Cre* knock-in mice, Jackson Laboratory Stock No: 005628, and NuTRAP mice, Jackson Laboratory Stock No: 029899).

Data Availability

RNA seq and CUT&RUN seq data will be deposited and publicly available as of the date of publication. Accession numbers will be listed here pending publication. Any additional information required to reanalyze the data reported in this paper is available from the lead contact upon request. Supplemental tables will be available upon publication.

Animals

Emx1-IRES-*Cre* knock-in mice (Jackson Laboratory Stock No: 005628) and NuTRAP mice (Jackson Laboratory Stock No: 029899) were obtained from Jackson Laboratories. Female Emx1-IRES-*Cre* and male NuTRAP mice were crossed to generate

the Emx1-NuTRAP mice used for this study. Mice were given free access to food and water and lights were maintained on a standard 12-hour light/dark cycle. On postnatal day (P) 21, mice were weaned and pair-housed in either standard bedding cages or cages equipped with a running wheel. Only male mice were used for the studies performed. Experiments were conducted according to US National Institutes of Health guidelines for animal care and use and were approved by the Institutional Animal Care and Use Committee of the University of California, Irvine.

Exercise Paradigm

After weaning on P21, male mice from the same litters were randomly divided and pair-housed in either standard cages without a wheel or cages equipped with a stainless-steel running wheel similar to methods already described [17]. Animals housed with running wheels had free access to the wheels from P21–41. Real-time data acquisition (Vital View Software) was used to track distance ran recorded by magnetic sensors that detect wheel revolutions. Each monitored wheel tracked running distance for the entire cage (two mice per cage). Revolutions were quantified for every minute daily for the duration of the exercise period and converted to distance ran per cage (km).

Simultaneous RNA and Nuclear Isolation

On P42 both ELE (n=4) and sedentarycontrol (n=4) mice were sacrificed by rapid cervical dislocation and both hemispheres of the hippocampus were dissected out and collected for tissue processing. Hippocampal tissue samples were mechanically homogenized in 1mL of nuclear preparation buffer (NPB) (10mM HEPES (pH7.5);

1.5mM MgCl2; 10mM KCl; 250mM sucrose; 0.1% IGEPAL CA-630; 0.2mM DTT; 100µg/mL cycloheximide; 1x Complete EDTA-free protease inhibitor (Roche)). by razor blade. Samples were then triturated with an 18G needle and syringe 50x on ice.

Homogenized tissue samples were pipetted slowly onto 100µm cell strainer caps on 5mL tubes and centrifuged at 1,000rcf for 10 minutes at 4ºC. Cell pellets were resuspended and samples were pipetted onto 40µm cell strainer caps on 5mL tubes and centrifuged at 1,000rcf for 10 minutes at 4ºC. For nuclear isolation, 100µL of Streptavidin-coated Dynabeads were washed twice with 1mL NPB and resuspended with 100µL NPB. Cell pellets were resuspended and added to washed Streptavidin-coated Dynabeads. Samples were briefly pipetted to thoroughly suspend the beads and incubated on ice for 20 minutes. Samples were placed on a magnetic stand to pull down nuclei bound to the beads. The supernatant from each sample was slowly pipetted off the beads and transferred to new 1.5mL tubes for RNA isolation (described later). Nuclei-bound beads were washed twice with 1mL INTACT buffer (10mM HEPES (pH7.5); 1.5mM MgCl2; 10mM KCl; 250mM sucrose; 0.1% IGEPAL CA-630; 1x Complete EDTA-free protease inhibitor (Roche)) and resuspended in 100µL INTACT buffer. Bead-bound nuclei were flash frozen on dry ice and stored at -80ºC until ready for CUT&RUN chromatin digestion and DNA purification.

For RNA isolation, 100µL of concentrated TRAP isolation buffer (10mM HEPES pH 7.5; 117mM MgCl2; 1M KCl; 10% IGEPAL CA-630; 100µg/mL cycloheximide; 11mg/mL sodium heparin; 20mM DTT; 2.2units/µL Rnasin; 1x Complete EDTA-free protease inhibitor (Roche)) was added to each sample (suppernatant above). Samples were mixed by gentle pipetting and centrifuged at 16,000rcf for 10 minutes at 4ºC. The

supernatant from each sample was transferred to new 1.5mL tubes and 50µL of protein-G Dynabeads was added to each sample. (To bind anti-GFP, 100µL of protein-G Dynabeads were washed twice with 500µL NPB and resuspended to a final 100µL volume. 2µL anti-GFP antibody (Sigma-Aldrich, G6539, Lot:128M4867V) was added to each tube and incubated for 1 hour on a rotating nutator at 4ºC. Excess anti-GFP was washed off with 200µL NPB and beads were resuspended in a final 100µL volume.) Samples were incubated for 3h on a rotating nutator at 4ºC. Beads were washed 3x in 1mL high salt wash buffer (HSWB) (50mM Tris pH 7.5; 12mM MgCl2; 300mM KCl; 1% IGEPAL CA-630; 2mM DTT; 100 ug/mL cycloheximide) at 4ºC. After the third wash the beads were slowly resuspended in 350µL RLT buffer (from Qiagen RNeasy Mini kit #74004) by slowly pipetting up and down and incubated on a rotating nutator for 30 minutes at room temperature. Samples were placed on a magnetic stand to pull down the beads, and the supernatant from each were transferred to new 1.5mL tubes and stored at -80ºC until ready for RNA purification.

Separate TRAP RNA Isolation

On P42, mice (n=3) were sacrificed and the hippocampus was dissected out as described above. Either the left or right brain hemisphere of the hippocampus was processed for TRAP RNA isolation using methods similar to those previously described [28, 81] and the other hemisphere was processed for INTACT nuclear isolation (see below). Hippocampal tissue was homogenized with a motorized pestle in 1ml of TRAP homogenization buffer (50mM Tris, pH 7.5; 12mM $MgCl_2$; 100mM KCl; 1% NP-40; 100µg/ml cycloheximide; 1mg/ml sodium heparin; 2mM DTT; 0.2units/µl RNasin; 1x

Complete EDTA-free protease inhibitor (Roche)). Samples were centrifuged at 16,000rcf for 10 minutes at 4ºC. The supernatant from each sample was collected and incubated with 50µL of protein G Dynabeads (washed twice in TRAP homogenization buffer without RNasin or protease inhibitor). Samples were incubated for 30 minutes on a rotating nutator at 4ºC. Following the incubation, 100µL of anti-GFP bound protein-G Dynabeads was added to each sample. (To bind anti-GFP, 100µL of protein-G Dynabeads were washed twice with 500µL TRAP homogenization buffer without RNasin or protease inhibitor and resuspended to a final 100µL volume. 2µL anti-GFP antibody (Sigma-Aldrich, G6539, Lot:128M4867V) was added to each tube and incubated for 1 hour on a rotating nutator at 4ºC. Excess anti-GFP was washed off with 200µL TRAP homogenization buffer without RNasin or protease inhibitor and beads were resuspended in a final 100µL volume.) Samples were incubated for 3 hours on a rotating nutator at 4ºC. Beads were washed 3x in 1 mL HSWB at 4ºC. After the final wash, the beads were resuspended in 350µL RLT buffer (from Qiagen RNeasy Mini kit #74004) and incubated on a rotating nutator for 30 minutes at room temperature . Following the incubation, samples were transferred to new 1.5mL tubes and stored at -80ºC until ready for RNA purification.

Separate INTACT Nuclear Isolation

The remaining hippocampal hemisphere from each mouse (not used for TRAP RNA isolation above) was processed for INTACT DNA isolation using methods similar to those described [28, 82]. Tissue samples were quickly chopped with a razor blade, added to 1mL of INTACT buffer, and triturated with an 18G needle and syringe 50x on

ice. Samples were then added onto 100µm cell strainer caps on 5mL tubes and centrifuged at 1,000rcf for 10 minutes at 4ºC. Cell pellets were resuspended and samples were pipetted onto 40µm cell strainer caps and centrifuged at 1,000rcf for 10 minutes at 4ºC. 100µL of streptavidin coated Dynabeads (washed twice with 1 mL INTACT buffer) were added to each sample, and samples were incubated on ice for 20 minutes. After incubation, nuclei bound beads were washed twice with 1mL and resuspended in 100 µL INTACT buffer. Bead-bound nuclei were flash frozen on dry ice and stored at -80ºC until ready for CUT&RUN chromatin digestion and DNA purification.

RNA Purification and Sequencing Library Preparation

RNA was purified using the Qiagen RNeasy kit according to the manufacturer's protocol. After purification, RNA quantity and quality were checked using the Qubit RNA High Sensitivity assay and Agilent Bioanalyzer's Eukaryote Total RNA Pico assay, respectively, at the University of California, Irvine Genomics High Throughput Facility (UCI GHTF). Using an input of 15ng of total RNA, mRNA was isolated using NEXTFLEX Poly(A) Beads 2.0, and the mRNA sequencing libraries were generated using the NEXTFLEX Rapid Directional RNA-Seq Kit 2.0 according to the manufacturer's instructions. Final libraries were sent to the UCI GHTF for Qubit dsDNA High Sensitivity assay and the Agilent Bioanalyzer DNA High Sensitivity assay to determine the quantity and quality of the RNA-seq libraries, respectively. Libraries were sequenced at the UCI GHTF using 100bp paired end reads on a single lane of an Illumina NovaSeq6000 to a minimum sequencing depth of 50 million reads.

Cleavage Under Target and Release Using Nuclease (CUT&RUN)

For chromatin analysis, CUT&RUN was performed using the EpiCypher CUTANA CUT&RUN protocol with slight modifications similar to what has already been described [35]. Nuclei bound to beads were thawed and pulled down on a magnetic stand. The supernatant was removed and beads were resuspended in 200µL wash buffer (20mM HEPES pH 7.5; 150mM NaCl; 0.5mM spermidine; 1x Complete EDTA-free protease inhibitor (Roche)). Each sample was divided into three aliquots (50µL for anti-H3K27me3 (Cell Signaling Technologies, C36B11, Lot: 16), 100µL for anti-H4K8ac (Epicypher, 13-0047, Lot: 20202001-11), and 50 µL for anti-IgG control (Rabbit IgG Fisher Scientific, 026102)). Beads were pulled down on a magnetic stand, resuspended in 100µL wash buffer and incubated for 10 minutes at room temperature. After incubation the beads were pulled down, the supernatant was removed, and the beads were resuspended in 50µL ice cold antibody buffer (20mM HEPES pH 7.5; 150mM NaCl; 0.5mM spermidine; 0.001mM digitonin; 2mM EDTA; 1x Complete EDTA-free protease inhibitor (Roche)). 0.5µL of the appropriate antibody was added to each sample, and the samples were mixed by gentle pipetting prior to overnight incubation at 4ºC on a nutator.

On the second day, the beads were pulled down on a magnetic stand, the supernatant was removed and the beads were washed twice in 250µL ice cold wash buffer with 0.001% digitonin. After the washes, beads were resuspended in 50µL ice cold wash buffer with 0.001% digitonin, and 2.5µL of CUTANA pAG-MNase was added to each sample and mixed by gentle pipetting. Samples were incubated for 10 minutes at room temperature and beads were pulled down on a magnetic stand. The supernatant was

removed, and the beads were washed twice in 250µL ice cold wash buffer with 0.001% digitonin and resuspended in 50µL of the same. 1µL of 100mM $CaCl_2$ was added to each sample and mixed by gentle pipetting. Samples were incubated for 2 hours on a nutator at 4ºC. Following the incubation, 33µL of stop buffer (340mM NaCl; 20mM EDTA; 4mM EGTA; 50µg/mL RNase A; 50µg/mL Glycogen) and 1.65µL of Spike-In DNA (Cell Signaling Technology, #40366) was added to each sample. Samples were incubated in a preheated thermocycler for 10 minutes at 37ºC. After incubation, samples were transferred to new 1.5mL tubes and immediately processed for DNA purification.

DNA Purification and Library Preparation

DNA was purified using the Monarch PCR and DNA cleanup kit (New England Biolabs, 13-0041) according to the manufacturer's instructions. After purification, DNA fragments were used to generate sequencing libraries using the NEXTFLEX Rapid DNA-Seq Kit 2.0 according to the manufacturer's instructions. Indices were diluted to a final concentration of 1:1,000 before being added to samples, and a total of 13 PCR cycles was used for DNA amplification of the libraries. Final libraries were sent to the UCI GHTF for Qubit dsDNA High Sensitivity assay and the Agilent Bioanalyzer DNA High Sensitivity assay to determine the quantity and quality of the CUT&RUN-seq libraries, respectively. Libraries were sequenced at the UCI GHTF using 100bp paired end reads on a single lane of an Illumina NovaSeq6000 to a minimum sequencing depth of 10 million reads.

qPCR

cDNA was generated from TRAP-isolated and total input RNA samples using the Transcriptor First Strand cDNA Synthesis Kit (Roche) following the manufacturer's instructions. Relative gene expression for *Aqp4* (F: 5'-ATCCAGCTCGATCTTTTGGA -3', R: 5'-TGAGCTCCACATCAGGACAG -3'), *Tubb3* (F: 5'-GTCTCTAGCCGCGTGAAGTC -3', R: 5'-GCAGGTCTGAGTCCCCTACA -3'), *Cd11b* (F: 5'-CCCATGACCTTCCAAGAGAA -3', R: 5'-ACACTGGTAGAGGGCACCTG -3'), and *Mog* (F: 5'-AAGAGGCAGCAATGGAGTTG -3', R: 5'-GACCTGCAGGAGGATCGTAG -3') was determined by qPCR using FastStart Essential DNA Green Master Mix (Roche, 06402712001) following the manufacturer's protocol. Cycle counts for mRNA quantification were normalized to *Gapdh* (F: 5'-CGTCCCGTAGACAAAATGGT -3', R: 5'-GAATTTGCCGTGAGTGGAGT -3'). Quantification was performed using the Pfaffl method [83].

Immunofluoresence

Emx1-NuTRAP mice were anesthetized intraperitoneally with 50mg/kg of sodium pentobarbital and transfused transcardially with 4% paraformaldehyde (PFA) in 1x PBS. After perfusion, whole brains were dissected out and incubated in 4% PFA overnight at 4ºC. After fixation, brains were incubated in 30% sucrose for 72 hours and mounted in optimal cutting temperature (OCT) compound. 50µm coronal sections were sliced through the hippocampus using a microtome, and every tenth section was collected in 1mL of cryoprotectant and stored at -20ºC until ready for immunofluorescent labeling. For immunofluorescence, sections were brought up to room temperature and washed 2x

in 1x PBS on a nutator for 5 minutes each. Sections were then washed 3x in 1x PBS with 0.3% triton-X. After washes, sections were incubated with mCherry polyclonal antibody (ThermoFisher, PA5-34974, Lot: UG2804409F) at a 1:200 dilution in blocking solution (1x PBS with 1% BSA) overnight at 4ºC on a nutator. The following day, sections were washed 3x in 1x PBS. Sections were incubated for two hours at room temperature with goat anti-rabbit Alexa Fluor 594 secondary antibody (Invitrogen, A-11012, Lot: 2119134) at a 1:200 dilution in blocking solution. After incubation, the sections were washed twice in 1x PBS. To label nuclei, sections were incubated with DAPI at a 1:10,000 dilution in 1x PBS for 20 minutes. Sections were then washed 3x in 1x PBS and cover slipped with Vectatshield®. Fluorescent images were acquired using a Keyence BZ-X810 All-in-One Fluorescence microscope using the optical sectioning module.

Fluorescence Activated Cell Sorting

Whole hippocampal tissue from Emx-NuTRAP mice was isolated and fluorescence activated cell sorting (FACS) using an Aria Fusion from the University of California, Irvine Stem Cell Core was performed to characterize neuronal and astrocytic NuTRAP cassette expression using methods similar to what has been described [84]. We used antibodies for THY-1(Santa Cruz Biotechnology, sc-53116 AF647, Lot: F2716; concentration: 1:50) and S100β (Abcam, ab41548, Lot:GR3326165-1; concentration: 1:200) with a AlexaFluor™ 405 goat anti-rabbit IgG (H+L) (Invitrogen, A31556, Lot: 2273716; concentration:1:800).

Bioinformatics Analysis

Reference assembly: For all sequencing analysis that required it, the primary reference assembly used was Genome Reference Consortium Mouse Build 38 patch release 6 (GRCm38.p6).

RNA-seq analysis: FastQ files were quality checked for sequencing errors using FastQC (version 0.11.9)[85]. No files were found to have sufficient quality errors to discount their use. Files were aligned using STAR Aligner (version 2.7.3a) [86]. Duplicate reads were removed using Picard Tools (version 1.87) [87]. SAM Tools was used to convert BAM files to SAM files for use in downstream analysis. FastQC, alignment and duplicate removal were all preformed on the High-Powered Compute Cluster (HPC3) operated by The Research Cyberinfrastructure Center (RCIC) at the University of California, Irvine (UCI). R (version 4.1.0) [88] was used for differentially expressed genes (DEG) analysis. Genomic Alignments (version 1.28.0) [89] (summarizeOverlaps mode="IntersectionNotEmpty", singleEnd=FALSE, ignore.strand=FALSE, fragments=TRUE), Genomic Features (version 1.44.0) (exons by gene), and R SAM Tools (version 2.8.0) [90] (yieldSize=100000) were used to extract a count matrix and generate a summarized experiment object. DEseq2 (version 1.32.0) [91] was used to perform a DEG analysis. Ensemble IDs were converted to gene symbols using BiomaRt (version 2.48.1) [92, 93]. PCA plots using the top 2000 genes were generated using ggplot2 (version 3.3.4) [94]. Samples were determined as outliers if a PCA plot that included them showed that most of the difference between the samples was represented by those samples deemed outliers alone (3 samples). Heatmaps were generated using gplots (version 3.1.1) [95] and RColorBrewer (version1.1-2) [96]. Volcano Plots were generated using ggplot2

[94]. Venn diagrams were generated using the Venn diagram tool from Bioinformatics and Evolutionary Genomics [97]. Gene ontology analysis was performed using Panther Classification System (version 16.0) [41]. Genes were also categorized and a leading edge heatmap was also generated using Gene Set Enrichment Analysis (version GSEA 4.1.0) [52]. Upstream regulators were identified from the DEGs upregulated by ELE using Qiagen's Ingenuity Pathway Analysis (IPA) (Fall 2021 Release) [42].

CUT&RUN-seq analysis: FastQ files were quality checked for sequencing errors using FastQC (version 0.11.9) [85]. No files were found to have sufficient quality errors to discount their use. FastQ files were aligned using Bowtie2 (version 2.4.1) [98]. Significant peaks were called from these aligned files using SEACR, developed in CUT&Tag for efficient epigenomic profiling of small samples and single cells [58, 98], according to CUT&Tag Data Processing and Analysis Tutorial (updated August 12 2020): https://www.protocols.io/view/cut-amp-tag-data-processing-and-analysis-tutorial-bjk2kky. An FDR higher than 0.1 was considered too high for called peaks. This threshold excluded 4 samples. Peaks were called using the stringent and 0.01 settings. Significant peaks were annotated using ChIPseeker (version 1.8.6) [99] using TxDb.Mmusculus.UCSC.mm10.knownGene [100] as a reference with the following settings: tssRegion = c(-3000, 3000), TxDb = TxDb.Mmusculus.UCSC.mm10.knownGene, level = "transcript", assignGenomicAnnotation = TRUE, genomicAnnotationPriority = c("Promoter", "5UTR", "3UTR", "Exon", "Intron", "Downstream", "Intergenic"), annoDb = NULL, addFlankGeneInfo = FALSE, flankDistance = 5000, sameStrand = FALSE,

ignoreOverlap = FALSE, ignoreUpstream = FALSE, ignoreDownstream = FALSE, overlap = "TSS", verbose = TRUE). This approach annotated peaks to the closest gene by distance from the promoter, except if that peak falls within a gene before the distal intergenic region. Ensemble IDs were converted to gene symbols using BiomaRt [92, 93]. Gene lists of peaks present in each condition were used to generate Venn diagrams, as with RNA-seq analysis[97]. Further Venn diagrams were generated comparing DEGs with peak calls. Peaks were visualized using UCSC Genome Browser and Genome Browser in a Box [101-103].

Normalized counts (for read depth) at binned sections of the DNA as well as RNA-seq gene expression count (normalized for read depth) were compared between simultaneous and separate isolations as well as left and right hemispheres using spearman correlations in R with the package ggpubr (version 0.4.0) [104]. Bar plots were generated using Graph Pad 9 PRISM.

References

1. Bedrosian, T.A., et al., *Early life experience drives structural variation of neural genomes in mice.* Science, 2018. **359**(6382): p. 1395-1399.
2. Stroud, H., et al., *Early-Life Gene Expression in Neurons Modulates Lasting Epigenetic States.* Cell, 2017. **171**(5): p. 1151-1164.e16.
3. Herre, M. and E. Korb, *The chromatin landscape of neuronal plasticity.* Curr Opin Neurobiol, 2019. **59**: p. 79-86.
4. Campbell, R.R. and M.A. Wood, *How the epigenome integrates information and reshapes the synapse.* Nat Rev Neurosci, 2019. **20**(3): p. 133-147.
5. Kronman, H., et al., *Long-term behavioral and cell-type-specific molecular effects of early life stress are mediated by H3K79me2 dynamics in medium spiny neurons.* Nat Neurosci, 2021. **24**(5): p. 667-676.
6. Sagarkar, S., et al., *LSD1-BDNF activity in lateral hypothalamus-medial forebrain bundle area is essential for reward seeking behavior.* Prog Neurobiol, 2021. **202**: p. 102048.
7. Webb, W.M., et al., *The SETD6 Methyltransferase Plays an Essential Role in Hippocampus-Dependent Memory Formation.* Biological psychiatry, 2020. **87**(6): p. 577-587.
8. Bolton, J.L., et al., *Unexpected Transcriptional Programs Contribute to Hippocampal Memory Deficits and Neuronal Stunting after Early-Life Adversity.* Cell Rep, 2020. **33**(11): p. 108511.
9. Campbell, R.R., et al., *HDAC3 Activity within the Nucleus Accumbens Regulates Cocaine-Induced Plasticity and Behavior in a Cell-Type-Specific Manner.* The Journal of neuroscience : the official journal of the Society for Neuroscience, 2021. **41**(13): p. 2814-2827.
10. Lister, R., et al., *Global Epigenomic Reconfiguration During Mammalian Brain Development.* Science, 2013. **341**(6146): p. 1237905.
11. Lavery, L.A. and H.Y. Zoghbi, *The distinct methylation landscape of maturing neurons and its role in Rett syndrome pathogenesis.* Curr Opin Neurobiol, 2019. **59**: p. 180-188.
12. Aguilar, R., et al., *Epigenetic silencing of the osteoblast-lineage gene program during hippocampal maturation.* J Cell Biochem, 2021. **122**(3-4): p. 367-384.
13. West, A.E. and M.E. Greenberg, *Neuronal activity-regulated gene transcription in synapse development and cognitive function.* Cold Spring Harb Perspect Biol, 2011. **3**(6).
14. Bale, T.L., et al., *Early life programming and neurodevelopmental disorders.* Biol Psychiatry, 2010. **68**(4): p. 314-9.
15. Cotman, C.W., N.C. Berchtold, and L.-A. Christie, *Exercise builds brain health: key roles of growth factor cascades and inflammation.* Trends in Neurosciences, 2007. **30**(9): p. 464-472.
16. Voss, M.W., et al., *Bridging animal and human models of exercise-induced brain plasticity.* Trends Cogn Sci, 2013. **17**(10): p. 525-44.
17. Ivy, A.S., et al., *A Unique Mouse Model of Early Life Exercise Enables Hippocampal Memory and Synaptic Plasticity.* Scientific Reports, 2020. **10**(1): p. 9174.

18. Berchtold, N.C., N. Castello, and C.W. Cotman, *Exercise and time-dependent benefits to learning and memory.* Neuroscience, 2010. **167**(3): p. 588-97.
19. Urdinguio, R.G., et al., *Physical exercise shapes the mouse brain epigenome.* Mol Metab, 2021. **54**: p. 101398.
20. Abel, J.L. and E.F. Rissman, *Running-induced epigenetic and gene expression changes in the adolescent brain.* Int J Dev Neurosci, 2013. **31**(6): p. 382-90.
21. Ieraci, A., et al., *Physical exercise and acute restraint stress differentially modulate hippocampal brain-derived neurotrophic factor transcripts and epigenetic mechanisms in mice.* Hippocampus, 2015. **25**(11): p. 1380-92.
22. Intlekofer, K.A., et al., *Exercise and Sodium Butyrate Transform a Subthreshold Learning Event into Long-Term Memory via a Brain-Derived Neurotrophic factor-Dependent Mechanism.* Neuropsychopharmacology, 2013. **38**(10): p. 2027-2034.
23. Titterness, A.K., et al., *Voluntary exercise does not enhance long-term potentiation in the adolescent female dentate gyrus.* Neuroscience, 2011. **183**: p. 25-31.
24. Gomes da Silva, S. and R.M. Arida, *Physical activity and brain development.* Expert Rev Neurother, 2015. **15**(9): p. 1041-51.
25. Gomes da Silva, S., et al., *Early exercise promotes positive hippocampal plasticity and improves spatial memory in the adult life of rats.* Hippocampus, 2012. **22**(2): p. 347-58.
26. Fernandes, J., R.M. Arida, and F. Gomez-Pinilla, *Physical exercise as an epigenetic modulator of brain plasticity and cognition.* Neurosci Biobehav Rev, 2017. **80**: p. 443-456.
27. Butler, C.W., et al., *Exercise opens a temporal window for enhanced cognitive improvement from subsequent physical activity.* Learn Mem, 2019. **26**(12): p. 485-492.
28. Roh, H.C., et al., *Simultaneous Transcriptional and Epigenomic Profiling from Specific Cell Types within Heterogeneous Tissues In Vivo.* Cell Rep, 2017. **18**(4): p. 1048-1061.
29. Deal, R.B. and S. Henikoff, *The INTACT method for cell type-specific gene expression and chromatin profiling in Arabidopsis thaliana.* Nat Protoc, 2011. **6**(1): p. 56-68.
30. Heiman, M., et al., *A translational profiling approach for the molecular characterization of CNS cell types.* Cell, 2008. **135**(4): p. 738-48.
31. Gorski, J.A., et al., *Cortical excitatory neurons and glia, but not GABAergic neurons, are produced in the Emx1-expressing lineage.* J Neurosci, 2002. **22**(15): p. 6309-14.
32. Chan, C.H., et al., *Emx1 is a marker for pyramidal neurons of the cerebral cortex.* Cereb Cortex, 2001. **11**(12): p. 1191-8.
33. Willaime-Morawek, S. and D. van der Kooy, *Cortex- and striatum- derived neural stem cells produce distinct progeny in the olfactory bulb and striatum.* Eur J Neurosci, 2008. **27**(9): p. 2354-62.
34. Luo, L., et al., *Optimizing Nervous System-Specific Gene Targeting with Cre Driver Lines: Prevalence of Germline Recombination and Influencing Factors.* Neuron, 2020. **106**(1): p. 37-65.e5.

35. Skene, P.J., J.G. Henikoff, and S. Henikoff, *Targeted in situ genome-wide profiling with high efficiency for low cell numbers.* Nature Protocols, 2018. **13**(5): p. 1006-1019.
36. Liu, Y., et al., *Glial fibrillary acidic protein-expressing neural progenitors give rise to immature neurons via early intermediate progenitors expressing both glial fibrillary acidic protein and neuronal markers in the adult hippocampus.* Neuroscience, 2010. **166**(1): p. 241-51.
37. Garcia, A.D.R., et al., *GFAP-expressing progenitors are the principal source of constitutive neurogenesis in adult mouse forebrain.* Nature Neuroscience, 2004. **7**(11): p. 1233-1241.
38. Chucair-Elliott, A.J., et al., *Inducible cell-specific mouse models for paired epigenetic and transcriptomic studies of microglia and astroglia.* bioRxiv, 2019: p. 862722.
39. Berchtold, N.C., et al., *Exercise primes a molecular memory for brain-derived neurotrophic factor protein induction in the rat hippocampus.* Neuroscience, 2005. **133**(3): p. 853-61.
40. McNulty, S.E., et al., *Differential roles for Nr4a1 and Nr4a2 in object location vs. object recognition long-term memory.* Learn Mem, 2012. **19**(12): p. 588-92.
41. Mi, H. and P. Thomas, *PANTHER Pathway: An Ontology-Based Pathway Database Coupled with Data Analysis Tools*. 2009, Humana Press. p. 123-140.
42. Krämer, A., et al., *Causal analysis approaches in Ingenuity Pathway Analysis.* Bioinformatics, 2014. **30**(4): p. 523-530.
43. Kandel, E.R., *The molecular biology of memory: cAMP, PKA, CRE, CREB-1, CREB-2, and CPEB.* Molecular Brain, 2012. **5**(1): p. 14.
44. Kerimoglu, C., et al., *KMT2A and KMT2B Mediate Memory Function by Affecting Distinct Genomic Regions.* Cell Reports, 2017. **20**(3): p. 538-548.
45. Ashbrook, D.G., et al., *Transcript co-variance with Nestin in two mouse genetic reference populations identifies Lef1 as a novel candidate regulator of neural precursor cell proliferation in the adult hippocampus.* Front Neurosci, 2014. **8**: p. 418.
46. Tapia-González, S., et al., *Smad3 is required for the survival of proliferative intermediate progenitor cells in the dentate gyrus of adult mice.* Cell Communication and Signaling, 2013. **11**(1): p. 93.
47. Tiano, J.P., D.A. Springer, and S.G. Rane, *SMAD3 Negatively Regulates Serum Irisin and Skeletal Muscle FNDC5 and Peroxisome Proliferator-activated Receptor γ Coactivator 1-α (PGC-1α) during Exercise.* Journal of Biological Chemistry, 2015. **290**(12): p. 7671-7684.
48. Sun, Z., et al., *EGR1 recruits TET1 to shape the brain methylome during development and upon neuronal activity.* Nature Communications, 2019. **10**(1).
49. Bouché, V., et al., *Drosophila Mitf regulates the V-ATPase and the lysosomal-autophagic pathway.* Autophagy, 2016. **12**(3): p. 484-98.
50. Guan, Z., et al., *Integration of long-term-memory-related synaptic plasticity involves bidirectional regulation of gene expression and chromatin structure.* Cell, 2002. **111**(4): p. 483-93.

51. Korzus, E., M.G. Rosenfeld, and M. Mayford, *CBP Histone Acetyltransferase Activity Is a Critical Component of Memory Consolidation.* Neuron, 2004. **42**(6): p. 961-972.
52. Subramanian, A., et al., *Gene set enrichment analysis: A knowledge-based approach for interpreting genome-wide expression profiles.* Proceedings of the National Academy of Sciences, 2005. **102**(43): p. 15545-15550.
53. Nofrini, V., D. Di Giacomo, and C. Mecucci, *Nucleoporin genes in human diseases.* European Journal of Human Genetics, 2016. **24**(10): p. 1388-1395.
54. Gomes-Duarte, A., et al., *eIF3: a factor for human health and disease.* RNA Biol, 2018. **15**(1): p. 26-34.
55. Alvarez-López, M.J., et al., *Long-term exercise modulates hippocampal gene expression in senescent female mice.* J Alzheimers Dis, 2013. **33**(4): p. 1177-90.
56. Butler, A.A., et al., *O-GlcNAc and EZH2-mediated epigenetic regulation of gene expression during consolidation of fear memories.* Learning & memory (Cold Spring Harbor, N.Y.), 2019. **26**(9): p. 373-379.
57. Butler, A.A., et al., *O-GlcNAc and EZH2-mediated epigenetic regulation of gene expression during consolidation of fear memories.* Learn Mem, 2019. **26**(9): p. 373-379.
58. Kaya-Okur, H.S., et al., *CUT&Tag for efficient epigenomic profiling of small samples and single cells.* Nature Communications, 2019. **10**(1).
59. Stergiopoulos, A., M. Elkouris, and P.K. Politis, *Prospero-related homeobox 1 (Prox1) at the crossroads of diverse pathways during adult neural fate specification.* Front Cell Neurosci, 2014. **8**: p. 454.
60. Camp, N.D., et al., *Individual protomers of a G protein-coupled receptor dimer integrate distinct functional modules.* Cell Discov, 2015. **1**: p. 15011-.
61. Baple, E.L., et al., *Mutations in KPTN cause macrocephaly, neurodevelopmental delay, and seizures.* Am J Hum Genet, 2014. **94**(1): p. 87-94.
62. Peterson, M.D. and M.A. Titus, *F-actin distribution of Dictyostelium myosin I double mutants.* J Eukaryot Microbiol, 1994. **41**(6): p. 652-7.
63. Johnson Chacko, L., et al., *Transcriptome-Wide Analysis Reveals a Role for Extracellular Matrix and Integrin Receptor Genes in Otic Neurosensory Differentiation from Human iPSCs.* Int J Mol Sci, 2021. **22**(19).
64. Truter, S., et al., *Pro-alpha 2(V) collagen gene; pairwise analysis of the amino-propeptide coding domain, and cross-species comparison of the promoter sequence.* Connect Tissue Res, 1993. **29**(1): p. 51-9.
65. Lévy, J., et al., *EFNB2 haploinsufficiency causes a syndromic neurodevelopmental disorder.* Clin Genet, 2018. **93**(6): p. 1141-1147.
66. Xiong, C., et al., *Targeting Forward and Reverse EphB4/EFNB2 Signaling by a Peptide with Dual Functions.* Sci Rep, 2020. **10**(1): p. 520.
67. Zhu, F., et al., *EFNB2 facilitates cell proliferation, migration, and invasion in pancreatic ductal adenocarcinoma via the p53/p21 pathway and EMT.* Biomed Pharmacother, 2020. **125**: p. 109972.
68. Ferrari, K.J., E. Lavarone, and D. Pasini, *The Dual Role of EPOP and Elongin BC in Controlling Transcriptional Activity.* Mol Cell, 2016. **64**(4): p. 637-638.

69. Liefke, R., V. Karwacki-Neisius, and Y. Shi, *EPOP Interacts with Elongin BC and USP7 to Modulate the Chromatin Landscape.* Mol Cell, 2016. **64**(4): p. 659-672.
70. Jordan, J.T., *The rodent hippocampus as a bilateral structure: A review of hemispheric lateralization.* Hippocampus, 2020. **30**(3): p. 278-292.
71. Iwano, T., et al., *Prox1 postmitotically defines dentate gyrus cells by specifying granule cell identity over CA3 pyramidal cell fate in the hippocampus.* Development, 2012. **139**(16): p. 3051-62.
72. Luo, C., et al., *Single-cell methylomes identify neuronal subtypes and regulatory elements in mammalian cortex.* Science, 2017. **357**(6351): p. 600-604.
73. Skene, P.J., J.G. Henikoff, and S. Henikoff, *Targeted in situ genome-wide profiling with high efficiency for low cell numbers.* Nat Protoc, 2018. **13**(5): p. 1006-1019.
74. Helbling, J.-C., et al., *Combined Gene Expression and Chromatin Immunoprecipitation From a Single Mouse Hippocampus.* Current Protocols, 2021. **1**(2): p. e33.
75. Chucair-Elliott, A.J., et al., *Inducible cell-specific mouse models for paired epigenetic and transcriptomic studies of microglia and astroglia.* Commun Biol, 2020. **3**(1): p. 693.
76. Doty, R.W., et al., *Long-term reversal of hemispheric specialization for visual memory in a split-brain macaque.* Behav Brain Res, 1999. **102**(1-2): p. 99-113.
77. Duboc, V., et al., *Asymmetry of the Brain: Development and Implications.* Annu Rev Genet, 2015. **49**: p. 647-72.
78. Güntürkün, O., F. Ströckens, and S. Ocklenburg, *Brain Lateralization: A Comparative Perspective.* Physiol Rev, 2020. **100**(3): p. 1019-1063.
79. Hubel, D.H. and T.N. Wiesel, *Receptive fields, binocular interaction and functional architecture in the cat's visual cortex.* The Journal of Physiology, 1962. **160**(1): p. 106-154.
80. Spiers, H.J., et al., *Unilateral temporal lobectomy patients show lateralized topographical and episodic memory deficits in a virtual town.* Brain, 2001. **124**(Pt 12): p. 2476-89.
81. Long, J.Z., et al., *A smooth muscle-like origin for beige adipocytes.* Cell Metab, 2014. **19**(5): p. 810-20.
82. Deal, R.B. and S. Henikoff, *A simple method for gene expression and chromatin profiling of individual cell types within a tissue.* Dev Cell, 2010. **18**(6): p. 1030-40.
83. Pfaffl, M.W., *A new mathematical model for relative quantification in real-time RT-PCR.* Nucleic Acids Res, 2001. **29**(9): p. e45.
84. Schwarz, J.M., *Using fluorescence activated cell sorting to examine cell-type-specific gene expression in rat brain tissue.* J Vis Exp, 2015(99): p. e52537.
85. Andrews, S., *FastQC*, S. Andrews, Editor. 2005, Babraham Bioinformatics.
86. Dobin, A., et al., *STAR: ultrafast universal RNA-seq aligner.* Bioinformatics, 2013. **29**(1): p. 15-21.
87. Broad Institute, *Picard*. 2013, Broad Institute.

88. R Development Core Team, *R*. 2010, R Foundation for statistical Computing: Vienna, Austria. p. A language and environment for statistical computing.
89. Lawrence, M., et al., *Software for Computing and Annotating Genomic Ranges.* PLoS Computational Biology, 2013. **9**(8): p. e1003118.
90. Martin Morgan, H.P., Valerie Obenchain, Nathaniel Hayden, *Rsamtools: Binary alignment (BAM), FASTA, variant call (BCF), and tabix file import*. 2021, Bioconductor Bioconductor
91. Love, M.I., W. Huber, and S. Anders, *Moderated estimation of fold change and dispersion for RNA-seq data with DESeq2.* Genome Biology, 2014. **15**(12).
92. Durinck, S., et al., *BioMart and Bioconductor: a powerful link between biological databases and microarray data analysis.* Bioinformatics, 2005. **21**(16): p. 3439-3440.
93. Durinck, S., et al., *Mapping identifiers for the integration of genomic datasets with the R/Bioconductor package biomaRt.* Nature Protocols, 2009. **4**(8): p. 1184-1191.
94. Wickham, H., *Ggplot2: Elegant graphics for data analysis*, in *Use R!* 2016, Springer International Publishing: Cham, Switzerland.
95. Gregory R. Warnes, B.B., Lodewijk Bonebakker, Robert Gentleman, Wolfgang Huber, Andy Liaw, Thomas Lumley, Martin Maechler, Arni Magnusson, Steffen Moeller, Marc Schwartz, Bill Venables, Tal Galili, *gplots: Various R Programming Tools for Plotting Data*. 2020, Tal Galili
96. Neuwirth, E., *RColorBrewer: ColorBrewer Palettes*. 2014, Erich Neuwirth: CRAN.
97. Bioinformatics & Evolutionary Genomics, *Venn Diagram: Calculate and draw custom Venn diagrams*. 2021: BELGIUM.
98. Langmead, B. and S.L. Salzberg, *Fast gapped-read alignment with Bowtie 2.* Nature Methods, 2012. **9**(4): p. 357-359.
99. Humburg, P., et al., *ChIPseqR: analysis of ChIP-seq experiments.* BMC Bioinformatics, 2011. **12**(1): p. 39.
100. Bioconductor Core Team, B.P.M., *TxDb.Mmusculus.UCSC.mm10.knownGene: Annotation package for TxDb object(s)*. 2019, Bioconductor
101. Kent, W.J., et al., *The Human Genome Browser at UCSC.* Genome Research, 2002. **12**(6): p. 996-1006.
102. Rosenbloom, K.R., et al., *ENCODE whole-genome data in the UCSC Genome Browser.* Nucleic Acids Research, 2010. **38**(Database): p. D620-D625.
103. Haeussler, M., et al., *Navigating protected genomics data with UCSC Genome Browser in a Box.* Bioinformatics, 2014. **31**(5): p. 764-766.
104. Kassambara, A., *ggpubr: 'ggplot2' Based Publication Ready Plots*, A. Kassambara, Editor. 2020, CRAN.

Supplemental Figure 1

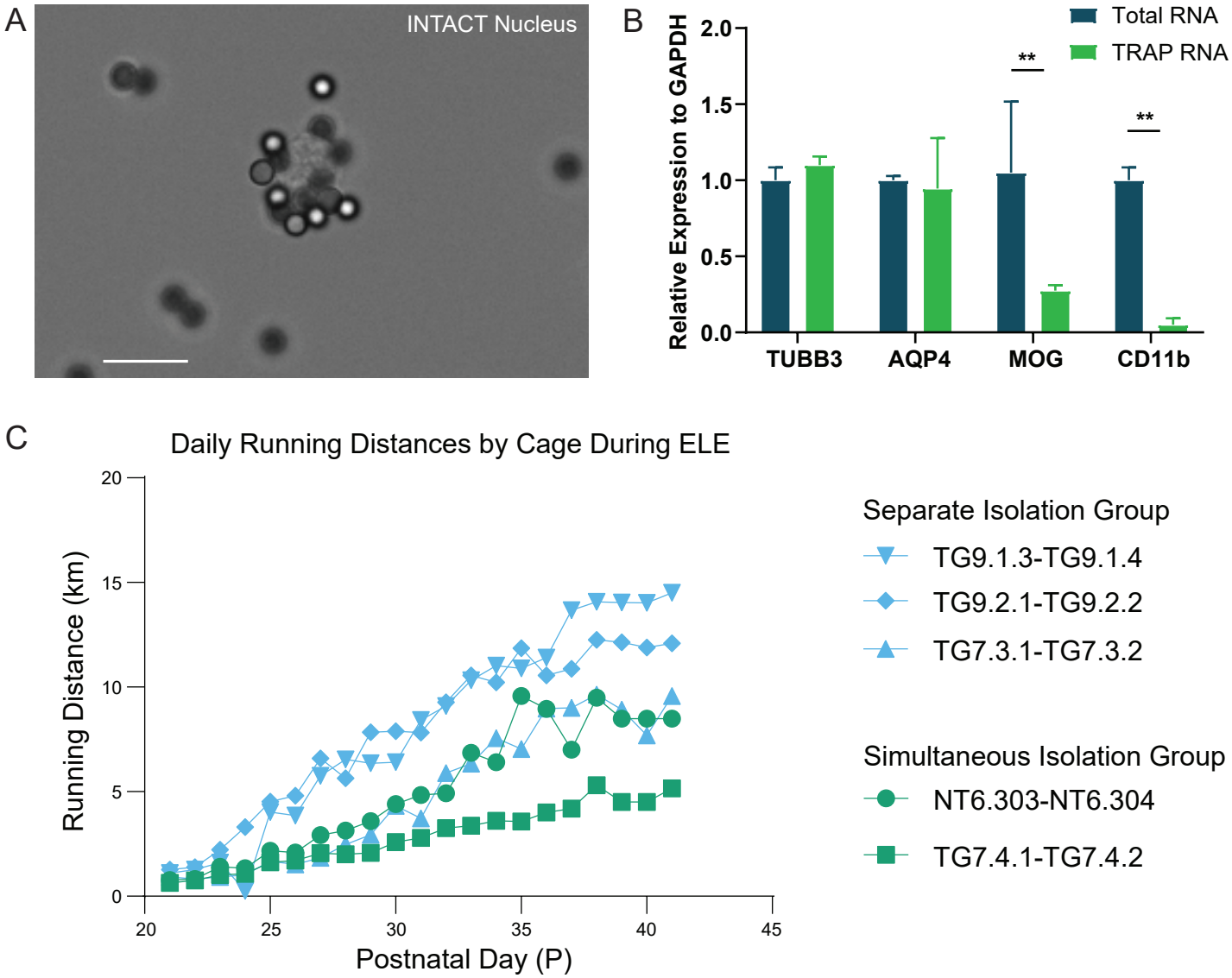

Supplemental Figure 1: (A) Brightfield microscopy of a neural nucleus bound to streptavidin coated Dynabeads™. The scale bar represents 10μm. (B) qPCR of TRAP isolated RNA compared to total RNA from the simultaneous isolation protocol **$p<0.01$. (C) Daily running distances of each cage during the ELE paradigm. Values of days missing or low due to software error were imputed by averaging the previous 3 days available. 2 Way Analysis of Variance (ANOVA) reveals that there is significant difference between postnatal days ($p<0.0001$) and cages ($p<0.0001$) but no significant effect of isolation ($p=0.1508$).

Supplemental Figure 2

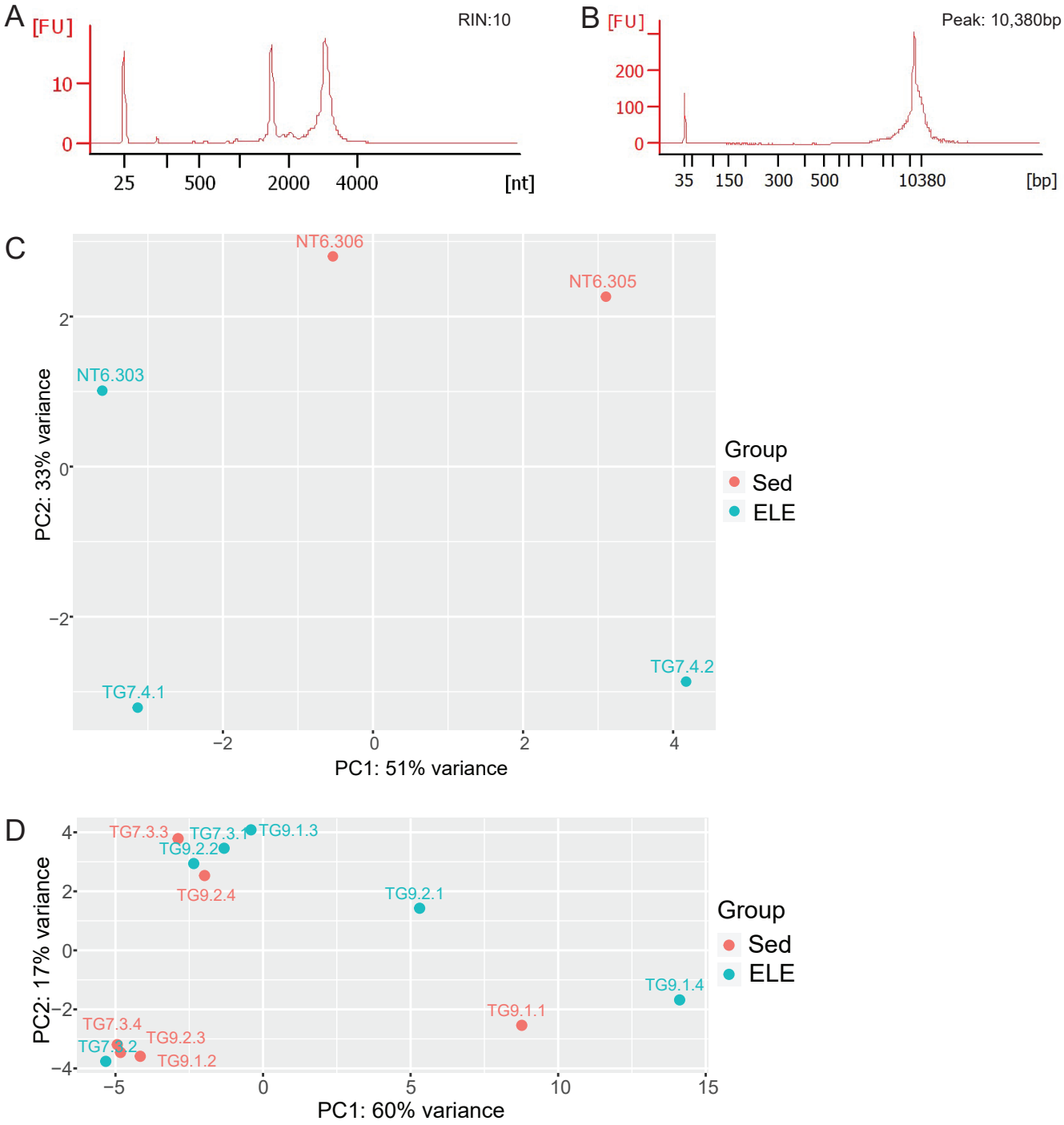

Supplemental Figure 2: (A) Representative electropherogram of RNA extracted using the simultaneous isolation protocol. (B) Representative electropherogram of DNA extracted using the simultaneous isolation protocol. (C) Principle component analysis plot (PCA) of RNA-seq data for the simultaneous isolations. (D) PCA of RNA-seq data for the separate isolations.

Supplemental Figure 3

A

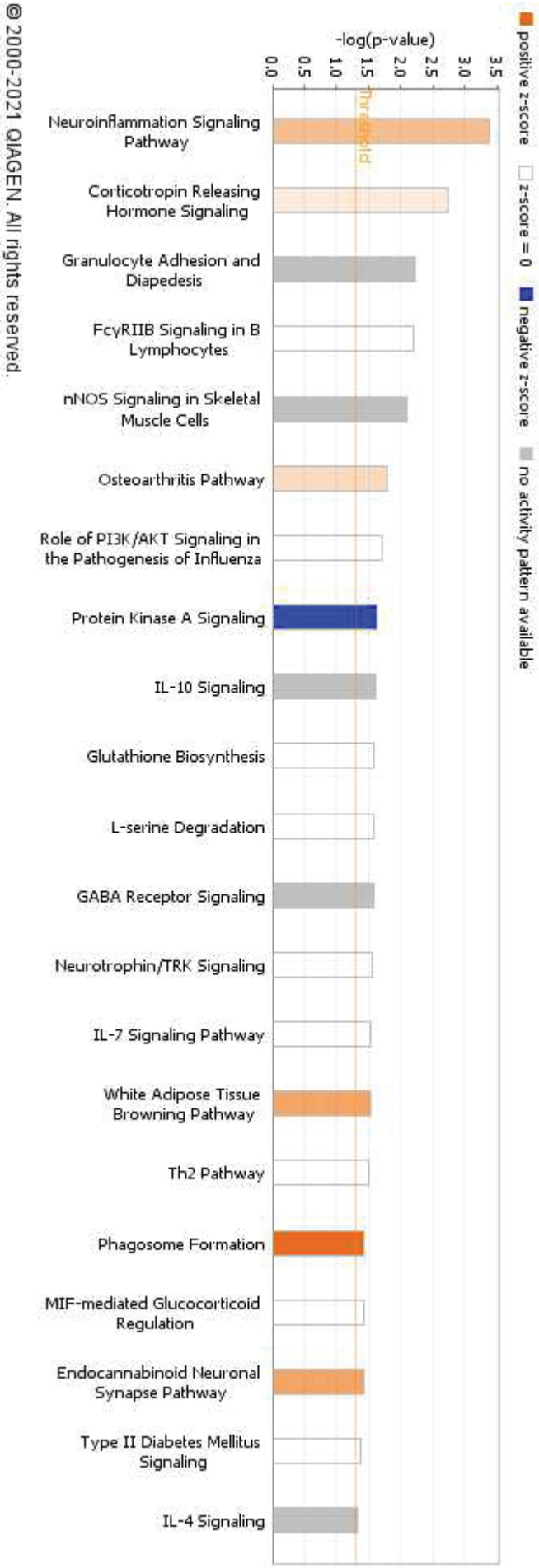

© 2000-2021 QIAGEN. All rights reserved.

Supplemental Figure 3: (A) Canonical pathways identified by Qiagen's IPA of genes upregulated by ELE. Supplemental table 3C and 3D have the genes identified by the top two pathways listed in this bar chart.